ARMY RESEARCH LABORATORY

Determination of Atmospheric Path Radiance: Sky-to-Ground Ratio for Wargamers

by Sean G. O'Brien and Richard C. Shirkey

ARL-TR-3285 **September 2004**

NOTICES

Disclaimers

The findings in this report are not to be construed as an official Department of the Army position, unless so designated by other authorized documents.

Citation of manufacturers' or trade names does not constitute an official endorsement or approval of the use thereof.

Army Research Laboratory
White Sands Missile Range, NM 88002-5501

ARL-TR-3285 **September 2004**

Determination of Atmospheric Path Radiance: Sky-to-Ground Ratio for Wargamers

Sean G. O'Brien and Richard C. Shirkey
Computational and Information Sciences Directorate

REPORT DOCUMENTATION PAGE

Form Approved
OMB No. 0704-0188

1. REPORT DATE *(DD-MM-YYYY)*	2. REPORT TYPE	3. DATES COVERED (From - To)
September 2004	Final	1996–2004

4. TITLE AND SUBTITLE
Determination of Atmospheric Path Radiance: Sky-to-Ground Ratio for Wargamers

5a. CONTRACT NUMBER

5b. GRANT NUMBER

5c. PROGRAM ELEMENT NUMBER

6. AUTHOR(S)
Sean G. O'Brien and Richard C. Shirkey

5d. PROJECT NUMBER

5e. TASK NUMBER

5f. WORK UNIT NUMBER

7. PERFORMING ORGANIZATION NAME(S) AND ADDRESS(ES)
U.S. Army Research Laboratory
Computational and Information Sciences Directorate
Battlefield Environment Division (ATTN: AMSRD-ARL-CI-EE)
White Sands Missile Range, NM 88002-5501

8. PERFORMING ORGANIZATION REPORT NUMBER
ARL-TR-3285

9. SPONSORING/MONITORING AGENCY NAME(S) AND ADDRESS(ES)
U.S. Army Research Laboratory
2800 Powder Mill Road
Adelphi, MD 20783-1145

10. SPONSOR/MONITOR'S ACRONYM(S)

11. SPONSOR/MONITOR'S REPORT NUMBER(S)
ARL-TR-3285

12. DISTRIBUTION/AVAILABILITY STATEMENT
Approved for public release; distribution is unlimited.

13. SUPPLEMENTARY NOTES

14. ABSTRACT
This document describes both the technical and user aspects of the sky-to-ground ratio program. The program computes sky-to-ground ratio, contrast transmission, transmission, path radiance, and zero-range-to-target background radiance for a user-specified observer (sensor) and target pair, situated on a slant path in the lower atmosphere for 19 different aerosols. Results are provided in hard-copy format and also in a computer-generated (tabular) file. The calculations are performed in one of three user-selectable bands: visible, mid-infrared, and far-infrared. Numerous examples are provided. A graphical user interface for this program is currently under development.

15. SUBJECT TERMS
Atmospheric, sky-to-ground ratio, path radiance, transmission, contrast, contrast transmission

16. SECURITY CLASSIFICATION OF:			17. LIMITATION OF ABSTRACT	18. NUMBER OF PAGES	19a. NAME OF RESPONSIBLE PERSON
a. REPORT	b. ABSTRACT	c. THIS PAGE	SAR	70	Richard C. Shirkey
U	U	U			19b. TELEPHONE NUMBER (*Include area code*) (505) 678-5470

Table of Contents

List of Figures

List of Tables

Preface

Target discrimination calculations are frequently based on a two-dimensional Johnson cycle criteria methodology and require characterizing the system by either minimum resolvable contrast or minimum resolvable temperature difference. For reflective sources and visual and near-infrared imaging systems the contrast of the target is reduced by path radiance (i.e., by background light or near-infrared radiation entering the line-of-sight to the target). Since determination of the path radiance is computationally intensive, many wargames use a related quantity called the sky-to-ground ratio. This ratio is an approximate method for representing the amount of diffuse radiation that is entering a user's line-of-sight. While codes that determine the sky-to-ground ratio have been in existence for some time, none of these codes consider the situation where the target might be some distance in front of the background, nor do they consider the infrared wavelength regions; those situations have been rectified here. Heretofore, atmospheric quantities, such as aerosol type, cloud base/height, and temperatures, have not been readily integrated into these types of codes. These quantities, and others, are now integral to this code and are available for selection by the user.

The authors would like to thank the Army Model and Simulation Office for providing seed money under the Army Model Improvement Program. We would also like to thank John Mazz (Army Materiel Systems Analysis Activity) and David Tofsted (U.S. Army Research Laboratory) for reviewing this report and providing helpful comments.

INTENTIONALLY LEFT BLANK.

Summary

The sky-to-ground ratio is often used in wargames as an approximate method for quantifying the amount of diffuse radiation that is entering a sensor's field of view. We may represent this quantity as $S_{gr} = I_{ps} / I_b(0)$, where I_{ps} is the limiting path radiance and $I_b(0)$ is the background radiance as seen at the target. These radiances, or diffuse radiation, act as "atmospheric noise" and reduce the apparent contrast when observing a target. However, computing the diffuse radiation field is not an easy task and usually requires research-grade computer codes. The delta-Eddington method, used herein for visible wavelength calculations, is an approximate method that assumes the angular dependence of the diffuse radiance can be represented by a polynomial linear in scattering angle. This method overcomes the large computer run times usually associated with determining the diffuse radiance in radiative transfer codes. At visible wavelengths, the aerosols found in the atmosphere frequently scatter radiation predominantly in the forward direction along the observer's line-of-sight. This highly peaked scattering further complicates the ability to predict the diffuse radiation, and the subsequent determination of the sky-to-ground ratio. One way that the calculation of the asymmetric scattering in the visible band can overcome this difficulty is by using the delta-Eddington approximation, which combines a Dirac delta function and a two-term approximation for the aerosol scattering function. At infrared wavelengths, scattering effects may be ignored in many situations and the computation of the sky-to-ground ratio is carried out by integrating the emission over the relevant lines-of-sight.

We have constructed a computer program that rapidly computes the sky-to-ground ratio in run times of less than one second. For visible wavelengths, we have modified the Fast Atmospheric Scattering computer code, and for infrared wavelengths, we have constructed new code. Both of the wavelength regimes have been wrapped into one code with supporting information on atmospheric aerosols and clouds, and integrated routines that allow for automatic determination of solar/lunar positions. The target/observer may be placed anywhere in the lower 5 km of the atmosphere and provisions have been made to allow the user to insert an optional sensor response curve. The program can be run interactively or in command-line batch mode, with output consisting of spectral, band-averaged, and band-integrated radiances, as well as the sky-to-ground ratio.

The program has been validated and caveats are presented to allow the user to avoid those areas where the approximations employed break down. We also present extensive examples of program use—specifically, a target being observed flying in a horizontal plane parallel to the ground surface. An example of the target looking downward at the observer is also presented. These scenarios are discussed in some detail in order to aid the user in understanding the geometries that may be encountered, in constructing the input file, and in interpreting the output information. "Canned" test cases are also provided for verification that the program is functioning correctly after a new installation.

1. Introduction

1.1 Overview

The sky-to-ground ratio (*1*, *2*) (hereafter referred to as SGR or S_{gr}) is used primarily in wargames as a method to quantify the amount of light scattered into a sensor's line-of-sight (LOS). This radiation results from multiple scattering processes that occur between light and particles that it encounters as it passes through the intervening atmospheric medium. Using research-grade radiative transfer codes, these atmospheric multiple scattering processes can be calculated "exactly" using many differing methods (*3–6*). However, such calculations, while fast, still take on the order of seconds, minutes, and depending upon the scenarios, even hours to perform. The Combined Arms and Support Task Force Evaluation Model (CASTFOREM) is an Army high-resolution, two-sided, force-on-force, stochastic systemic model of a combined arms conflict. Run times are scenario dependent and typically run approximately 1.5–1.7 hours (on a 2.2 GHz PC) per replication for a battalion-sized defensive scenario. Without smoke, the runs are approximately one-to-one. (*7*) Due to the stochastic nature of CASTFOREM, the treatment of time intensive physical processes, such as determination of atmospheric multiple scattering effects, must be kept to a minimum yet be physically accurate. This presents a quandary: accurate answers depend upon knowledge of physical processes (here, atmospheric scattering/emission), yet computer run time must be kept to a minimum to have wargames complete in reasonable clock time. Thus, the need exists for approximations such as the SGR.

This document presents a methodology for determining the SGR. The code, written in ANSI standard FORTRAN 90, is relatively fast running (~1 s on a 1 GHz PC for a typical scenario used in the validation and verification (V&V) section 5) and can be implemented directly into the wargame or used to construct lookup tables that can be accessed by the wargame. The code itself uses approximate methods for calculating the multiple scattering quantities that are used to determine the SGR. Limitations of the program are presented in section 10; it is suggested that the user peruse this section in order to avoid areas where the program's results may be questionable. Numerous options are available that allow the user to select various natural aerosols for global locations and times. Explanations of the SGR and other related quantities, to include an abbreviated explanation of the technique used, are presented herein. The code operates in the visible (0.35–0.75 μm), near-infrared (IR) (1.06 μm), mid-IR (3.0–5.0 μm), and far-IR (8.0–12.0 μm) spectral regions. Finally, for those individuals who are interested in the physics, the code has been liberally sprinkled with technical references.

1.2 Availability

The source code, written in ANSI FORTRAN 90 and C, is available by contacting either Dr. Sean O'Brien at (505) 678-1570 (sobrien@arl.army.mil) or Dr. Richard Shirkey at (505) 678-5470 (rshirkey@arl.army.mil). A graphical user interface (GUI) version of this code is under construction. Persons interested in such a version should contact Dr. Shirkey. Comments or questions relating to either the code or documentation (to include requests for electronic copies) may also be referred to the above persons.

2. The Sky-to-Ground Ratio

2.1 Theoretical Formulation: Visual Contrast

In order to acquire an object, one must be able to distinguish it from its background. This is the basic definition of contrast. Determining the contrast requires knowledge of the inherent radiance of the target and the background radiance at the target, where the target is usually considered to be at zero range (see fig. 1 for a pictorial representation of the following contrast quantities).

The inherent contrast (i.e. the contrast defined at zero range) is

$$C(0) = [\, I_t(0) - I_b(0) \,] \,/\, I_b(0), \tag{1}$$

where $I_t(0)$ is the target radiance at zero range (usually taken to be the location of the target) and $I_b(0)$ is the background radiance at zero range.

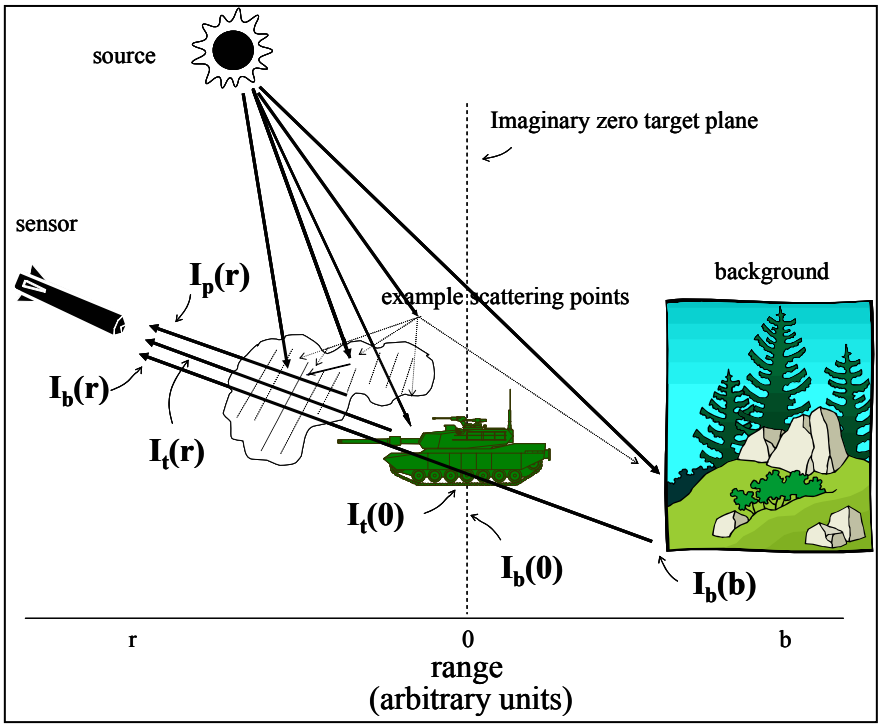

Figure 1. Pictorial representation of contrast quantities. $I_b(b)$ is the (inherent) background radiance at distance *b* from the target.

The radiance at range r can be represented by

$$I(r) = I(0)\, T(r) + I_p(r), \tag{2}$$

where I(0) is $I_t(0)$ or $I_b(0)$. T(r) is the transmission over the path r, given by $e^{-\kappa r}$, where κ is the extinction coefficient of the aerosol and/or gas comprising the intervening medium; $I_p(r)$ is the path

radiance over the path length r. The path radiance represents radiation emitted or scattered into the sensor's LOS and may be thought of as atmospheric noise, since it adds spurious information to the point or image being observed. The path radiance term is frequently the most difficult term to evaluate, requiring either approximate solutions or a research grade radiative transfer code.

Following eq 1, the apparent contrast is defined as

$$C(r) = [\ I_t(r) - I_b(r)\ ]/I_b(r). \tag{3}$$

Now, using eq 2, we can reformulate eq 3 as

$$\begin{aligned} C(r) &= [I_t(0)\ T(r) + I_p(r) - I_b(0)\ T(r) - I_p(r)] \,/\, [I_b(0)\ T(r) + I_p(r)] \\ &= [I_t(0) - I_b(0)] \,/\, [I_b(0) + I_p(r)/T(r)] \\ &= C(0)/\{1 + [I_p(r)/I_b(0)]\ T(r)^{-1}\}, \end{aligned} \tag{4}$$

where C(0) is the contrast at zero range, commonly referred to as the inherent contrast.

Because $I_p(r)$ is difficult and time consuming to calculate, approximations such as the SGR are frequently made in wargames to evaluate this term. Next, we derive the SGR approximation. In order to do this, we first must examine the radiative transfer equation

$$dI(r, \mathbf{\Omega}) / dr \ = \ - \kappa\ I(r,\mathbf{\Omega}) + \kappa\ [\varpi_o \textstyle\int_{\Omega'} I(r, \mathbf{\Omega'})\ P(\mathbf{\Omega},\mathbf{\Omega'})\ d\mathbf{\Omega'} + (\ 1 - \varpi_o)\ B(\lambda,t)], \tag{5}$$

where I is the radiance (in w/m^2-sr) at position *r* flowing in direction $\mathbf{\Omega}$; $I(r,\mathbf{\Omega'})$ is the angular distribution of the incoming radiation, which is being scattered into the direction in which the observer is looking ($\mathbf{\Omega}$); and $\varpi_\circ$ is the combined single scattering albedo for aerosols and gasses. $P(\mathbf{\Omega},\mathbf{\Omega'})$ is the phase function, which determines the angular probability of scattering from $\mathbf{\Omega'}$ into $\mathbf{\Omega}$, and $B(\lambda,t)$ is the Planck emission function at wavelength λ and temperature *t*. The term inside the square brackets is called the source term and includes diffuse and emitted radiation from all directions and sources.

Now consider the situation where the term in brackets is constant or slowly varying (i.e., an atmosphere homogeneous in the distribution of particulates and in illumination). Eq 5 can then be recast as

$$dI(r, \mathbf{\Omega}) / dr = \ - \kappa\ I(r,\mathbf{\Omega}) + \kappa\ A, \tag{6}$$

where

$$A = \varpi_\circ \textstyle\int_{\Omega'} I(r, \mathbf{\Omega'})\ P(\mathbf{\Omega},\mathbf{\Omega'})\ d\mathbf{\Omega'} + (\ 1 - \varpi_\circ\ )\ B(\lambda,t) \approx \text{constant}. \tag{7}$$

Using $e^{\kappa r}$ as an integrating factor for eq 6 and performing the integration over the path *r* from 0 to *s*, where *s* is large but not infinite, we find

$$I_s = I_0\ T + A\ (\ 1 - T\ ). \tag{8}$$

By comparing eq 8 with eq 2, we find

$$A = I_p / (1 - T) \quad \text{or} \quad I_p = A \ (1 - T). \tag{9}$$

Thus, as the transmission decreases, either through a longer path length or through an increased particle concentration, $I_p \rightarrow A$. When I_p reaches its limit A, we refer to it as the limiting path radiance I_{ps}, which is the point where radiation scattered into the LOS is equal to that scattered out of the LOS. Now using eq 9 in eq 4, we find that, under the conditions of limiting path radiance

$$T_c = \frac{C(r)}{C(0)} = \frac{1}{1 + [I_{ps} / I_b (0)](1 / T - 1)} = \frac{1}{1 + S_{gr}(1 / T - 1)}, \tag{10}$$

where T_c is the contrast transmission and

$$S_{gr} = I_{ps} \ / I_b(0) = I_p / [I_b(0) \ (1\text{-}T)], \tag{11}$$

which is the so-called sky-to-ground ratio. Thus, if S_{gr} is known, then we have a very quick, albeit approximate, means of calculating the apparent contrast.

2.2 Discussion

In deriving the SGR, the term in brackets in eq 5 requires that the intervening medium remain relatively constant. Slant paths in the atmosphere frequently traverse regions of inhomogeneities; horizontal paths also contain random fluctuations in the particle concentration and type. Nevertheless, the significance of this approach is that the concepts of inherent contrast and contrast transmission allow for the separation of target effects from atmospheric effects, which can be characterized in terms of the transmission and the sky-to-ground ratio. (*8*) In addition, one should not try to compare contrast transmission with transmission. Contrast transmission is a measure of the loss of contrast, and though it is a function of both path radiance and transmission, it should be thought of as a separate quantity propagated through the atmosphere. Transmission should be regarded simply as a loss of energy due to atmospheric propagation. Stated another way, increasing the gain of a sensor can compensate for the energy losses due to transmission alone, but cannot compensate for loss of contrast due to the additional path radiance signal that is present in the contrast transmission depiction of events. Of course, one may adjust the sensor threshold so that signal levels below that of the path radiance signal level are rejected, and that increased gain on the remaining target and background signals can restore the intrinsic contrast. This practice will also generally introduce additional radiance noise into the signals, thereby degrading the results. See also the discussion in the example section (section 9).

We now examine the behavior of the SGR function, eq 11. Since SGR is a function of three variables (path radiance, background radiance, and transmission) and these three variables are primarily a function of the aerosol particulate properties in the visible band, we cannot unequivocally predict the behavior of SGR. This assertion becomes clearer when we consider that, in general, as the particle size approaches and exceeds the wavelength, the proportion of radiation scattered into the forward direction increases, thereby increasing the amount of path and background radiance. On the other hand, path transmission is directly affected by the amount of radiation that the particle absorbs or scatters in all directions, which are functions of the aerosol particle single-scattering albedo. In the visible band of the spectrum, for fixed background radiance $I_b(0)$ and transmission T, the scenario illumination geometry strongly affects the value of

SGR, particularly in the case of larger aerosols. Such is not the case in the IR spectral band, where the dominant attenuation mechanism is usually absorption, which does not depend on the source-target-observer geometry.

When SGR = 1, the limiting path radiance is equal to the background radiance at the target position, and the path transmission T and the contrast transmission T_c are equal. This situation is encountered for horizontal paths in a plane-parallel atmosphere, where the background radiance is from a uniform, semi-infinite path, also known as the "horizon sky." With increasing distance from the observer, the transmission T over the horizon sky path eventually falls to a very low value and the path radiance that is observed as $I_b(0)$ is also equal to the limiting path radiance. As the limiting path radiance is approached at large optical depths along the horizon sky path, the radiance scattered into the LOS, along each additional path increment, is offset by the radiance that is scattered out of the LOS on the trip from that path segment back to the observer (equilibrium has been established).

When SGR > 1, the background radiance at the target position is lower than the limiting path radiance, which can be described as a "dark" or "cold" background scenario. This condition may be encountered for a LOS that has a low albedo surface as a background at a short distance behind the target. It may also be encountered in a clear, vertically inhomogeneous plane-parallel atmosphere for an upward slant path that looks from a sensor at low-altitude to a high-altitude target. In that event, the limiting path radiance (derived from the LOS path radiance and transmission) will include contributions from the dense lower atmosphere. The background radiance will only include contributions from the tenuous upper atmosphere, and may be considerably lower than the limiting path radiance.

When SGR < 1, a "bright" or "hot" background situation pertains where the background radiance is larger than the limiting path radiance. This condition may be encountered for downward LOS geometries where both the observer and target are at high altitudes (so that the limiting path radiance is low), for high albedo backgrounds (relative to the single-scattering aerosol albedo), or for (in the IR band) high-temperature backgrounds.

For both cases where SGR ≠ 1, the contrast transmission for a given LOS path will approach unity when the path transmission T approaches unity and will approach a value of T / S_{gr} as the path transmission T approaches 0. In all cases, T_c will take on values between 0 and unity.

3. Solutions for Visible Wavelengths: The Eddington and delta-Eddington Methodologies

In the visible band, where scattering is the primary contributor to LOS path radiance, an enhanced version of the U.S. Army Electro-Optic Systems Atmospheric Effects Library (EOSAEL) Fast Atmospheric Scattering (FASCAT) (*9*) delta-Eddington model is used. Because the underlying plane-parallel methodology used in this model is presented over various other documents (*9–13*), we present only a basic review here.

Determining contrast along a sensor's LOS requires solving the equation of transfer (eq 5). At visual wavelengths, the contribution to the source term from thermal emission $(1 - \varpi_\circ)B(\lambda,t)$ is negligible, and we can recast eq 5 as

$$\mu dI(\tau,\mu,\phi)/d\tau=-I(\tau,\mu,\phi)+\varpi_\circ /4\pi[\int_0^{2\pi}\int_{-1}^{+1} I(\tau,\mu',\phi')P(\mu,\phi;\mu',\phi')d\mu' d\phi'+\varpi_\circ/4(F_0P(\mu,\phi;\mu_0,\phi_0)e^{-\tau/\mu_0})], \quad (12)$$

where θ denotes the inclination to the outward normal (i.e., zenith angle), φ is the azimuth angle, $d\Omega = d\mu\, d\varphi$, $\mu = \cos\theta$, $\tau = \int \kappa\, r\, dr$, and πF_0 is the solar irradiance perpendicular to the direction of incidence.

Using the Eddington and delta-Eddington methodologies, we shall examine solutions to eq 12 in sections 3.1, 3.2, 3.3.

3.1 The Eddington Approximation

Eddington's approximation assumes that the angular dependence of the diffuse radiance can be represented by a polynomial linear in μ

$$I(\tau,\mu) = I_0(\tau) + I_1(\tau)\, \mu. \quad (13)$$

Because we have a determined intensity distribution, we have a priori fixed the phase function—a constant plus a cosine dependence. If we assume that the phase function can be expanded in terms of Legendre polynomials (*11*), substitute eq 13 into eq 12, and then integrate over θ and φ, we find that the only terms that do not integrate to 0 are of order 0 and 1. Thus, the phase function can be approximated by a two-term Legendre expansion (equivalent to the Henyey-Greenstein phase function truncated at the first term, i.e. $P_{HG} = 1 + 3g\cos\theta$)

$$P(\Theta) = \sum_l \omega_l P_l(\cos\Theta) = 1 + \omega_1(\tau)\cos\Theta, \quad (14)$$

where P_l are the Legendre polynomials, ω_l are the coefficients,

$$\cos\Theta = \mu\mu' + (1-\mu^2)^{1/2}(1-\mu'^2)^{1/2}\cos(\phi-\phi'), \quad (15)$$

and Θ is the angle between incident (primed) and scattered (unprimed) radiances.

While not particularly realistic (*14*), this linearly anisotropic phase function allows us to obtain equations for I_1 and I_0

$$dI_1/d\tau = -3(1-\varpi_\circ)I_0 + .75\varpi_\circ F_0 e^{-\tau/\mu_0}, \quad (16)$$

$$dI_0/d\tau = (1-\varpi_\circ g)I_1 + .75\varpi_\circ g\mu_0 F_0 e^{-\tau/\mu_0}, \quad (17)$$

where the asymmetry factor, g, is defined as $g = \frac{1}{2}\int_{-1}^{+1} P(\Theta)\cos\Theta\, d(\cos\Theta) = \omega_1/3$. Eqs 16 and 17 can be solved for the special case of a homogeneous layered atmosphere (*10*), where $\varpi_\circ$ and g are constant within each layer, but vary from layer to layer.

3.2 The Delta Approximation

When the scattering particles are large compared to the wavelength, such as at visible wavelengths, light is predominantly scattered in the forward direction. The mathematical formulation for this is represented by a highly peaked phase function where a large portion of the scattering occurs in a relatively small cone centered on 0º (the forward peak). The delta method represents the phase function as a Dirac delta function coupled with a phase function p' that has a reduced forward peak

$$P(\Theta) = 2f\,\delta(1-\cos\Theta) + (1-f)\,p'(\Theta), \tag{18}$$

where f is the fraction of energy scattered into the forward direction cone. We thus assume that radiation scattered into the forward peak is treated as unscattered, and appropriately reduce the optical thickness of the medium under consideration (*11*, *14–16*). This is equivalent to replacing the real medium by an equivalent one with a scattering coefficient

$$\kappa'_s = (1 - f)\,\kappa_s; \tag{19}$$

keeping the absorption constant $\kappa'_a = \kappa_a$, the single scattering albedo can be represented as

$$\varpi'_\circ = \varpi_\circ\,(1 - f)/(1 - \varpi_\circ\, f). \tag{20}$$

Thus, the total extinction coefficient becomes

$$\kappa' = (1 - \varpi_\circ\, f)\,\kappa. \tag{21}$$

Choosing the angle θ_o at which to truncate the phase function becomes a somewhat arbitrary choice. This angle is usually chosen as the point where the phase function begins to rapidly increase; the phase function is generally linearly interpolated from θ_o to 0º maintaining the slope of the untruncated phase function at θ_o. This is shown as a dashed line in figure 2. The gray portion shown in figure 2 is that portion of the phase function that is now considered to be incorporated into the direct beam. In the SGR program, θ_o has been set to 25º.

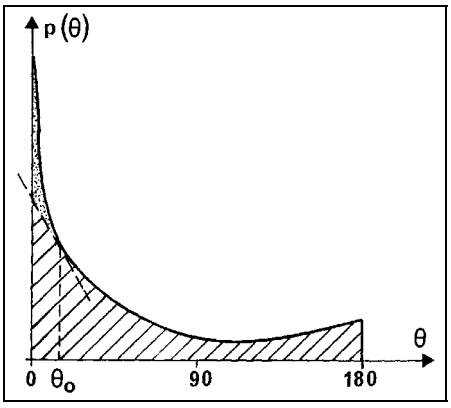

Figure 2. Truncation of phase function, after Lenoble (*16*).

We also note that while fog and cloud particles are all large with respect to visible wavelengths, and thus are in harmony with the above assumptions for the delta approximation, background aerosols (such as the rural, urban, and maritime aerosols) have significant contributions by particles less than 1 micron in diameter and could be construed as violating the aforementioned assumptions. Joseph, et. al. (*11*), and Wiscombe and Joseph (*17*) have shown that errors associated with the Eddington and delta-Eddington methods occur primarily when the incident radiation is impinging at large zenith angles or when the single-scattering albedo is near 0.5.

3.3 The delta-Eddington Approximation

For phase functions that are highly peaked in the forward direction (0º), the Eddington method is inaccurate. To overcome the difficulties in dealing with such highly asymmetric phase functions, Joseph, et. al.(*11*), have shown that by combining a Dirac delta function and a two-term approximation for the phase function, one can produce results that are more accurate. Such an approach has been called the delta-Eddington approximation. In this approximation, the phase function ($P_{\Delta E}$) is represented by

$$P_{\Delta E}(\cos\Theta) = [2f\delta(1-\cos\Theta) + (1-f)(1+3g'\cos\Theta)]\ 1/4\pi. \qquad (22)$$

The first term represents scattering in the forward direction (in essence, increasing the direct beam) and the second term represents a diffuse term. The parameter *f* determines the fraction of radiation scattered into the forward peak and g' is the asymmetry in the diffuse portion of the scattering function. Thus, when we have a highly peaked phase function, we may use the Eddington method by transformation of variables. According to van de Hulst (*18*), "Scattering in the exact forward direction is no scattering at all. Hence, if in any problem we add the formal assumption that a certain amount of scattering occurs in the exact forward direction, this must make no difference in the results." The proper transformation of variables is determined by requiring that the phase function meet certain conditions. Following Joseph, et. al. (*11*), it is required that the integral of eq 22 over θ be normalized to 1, and it is further required that the asymmetry factor be the same as in the Eddington method, which leads to

$$g = \tfrac{1}{2}\int_{-1}^{+1} P(\Theta)\cos\Theta\ d(\cos\Theta) =$$

$$\tfrac{1}{2}\int_{-1}^{+1} [2f\delta(1-\cos\Theta) + (1-f)(1+3g'\cos\Theta)]\cos\Theta\ d(\cos\Theta) = f + (1-f)\ g', \qquad (23)$$

where cosΘ is defined by eq 15. Finally, the second moments of the Eddington and the delta-Eddington phase functions are required to be equal (*11*), resulting in $f = g^2$.

Inserting eq 23 into the azimuthally averaged transfer equation, viz,

$$\mu\ dI(\tau,\mu')/d\tau + I(\tau,\mu') = \varpi_\circ \tfrac{1}{2}\int_{-1}^{+1} P(\mu,\mu')\ I(\tau,\mu')\ d\mu' = \varpi_\circ \tfrac{1}{2}\int_{-1}^{+1} [2f\delta(\mu-\mu') + (1-f)(1+3g'\mu\mu')]\ I(\tau,\mu')\ d\mu'$$

$$= \varpi_\circ f\ I(\tau,\mu') + \tfrac{1}{2}\ (1-f)\ \varpi_\circ\int_{-1}^{+1}(1+3g'\mu\mu')]\ I(\tau,\mu')\ d\mu', \qquad (24)$$

and $\mu = \cos\theta$, as before.

Rearranging eq 24 gives

$$\mu/(1-\varpi_\circ f)\ \ dI(\tau,\mu')/d\tau + I(\tau,\mu') = \tfrac{1}{2}\ \varpi_\circ\ (1-f)/(1-\varpi_\circ f)\int_{-1}^{+1}(1+3g'\mu\mu')\ I(\tau,\mu')\ d\mu'. \qquad (25)$$

Now, making the transformation of variables, $\tau' = (1-\varpi_\circ f)\ \tau$, and $\omega' = \varpi_\circ\ (1-f)\ /(1-\varpi_\circ f)$, eq 25 becomes

$$\mu\ dI(\tau',\mu')/d\tau' + I(\tau',\mu') = \tfrac{1}{2}\ \omega'\int_{-1}^{+1}(1+3g'\mu\mu')\ I(\tau',\mu')\ d\mu'. \qquad (26)$$

Eq 26 is now in a form where we can apply the Eddington method. It should be noted that, while eq 26 has no specific reference to the azimuthal angle ϕ, the code employs an extension of the Eddington methodology to handle an azimuthally dependent radiance field. (*19*)

4. Solutions for IR Wavelengths

4.1 Theoretical Formulation: IR Contrast

At IR wavelengths, scattering effects may be ignored in most cases and the equation of transfer takes the form

$$\mu dI(\tau,\mu,\phi)/d\tau = -I(\tau,\mu,\phi) + (\kappa_a/\kappa)\, B(\lambda,t), \tag{27}$$

where the total extinction coefficient (κ) is comprised of an absorption (κ_a) and scattering (κ_s) coefficient (i.e., $\kappa = \kappa_a + \kappa_s$), and we have made use of the fact that $\varpi_\circ = \kappa_s/\kappa$. It should be noted that each of the extinction coefficients may be broken into separate coefficients for aerosol and molecular components (i.e., $\kappa = \kappa_A + \kappa_M$); analogous expressions exist for κ_a and κ_s. The blackbody function (the Planck emission function) is given by

$$B(\lambda,t) = \frac{2\pi hc^2}{\lambda^5}\left[\frac{1}{e^{hc/\lambda kt}-1}\right], \tag{28}$$

where h is Planck's constant, k is Boltzmann's constant, and c is the speed of light in vacuum. Assuming a homogeneous atmosphere, we can integrate eq 27

$$I(\tau) = I(0)\, e^{-\tau/\mu} + (\kappa_a/\kappa)\, B\, (1 - e^{-\tau/\mu}). \tag{29}$$

In practice, because the atmosphere is not homogeneous, we use the numerical form

$$I(\tau) = \sum_{i=1}^{N} B_i e^{-\tau_i/\mu}\, \Delta\tau_i, \tag{30}$$

where B_i is the blackbody function for path segment; i, $e^{-\tau_i/\mu}$ is the total path transmission between segment i and the observer; and $\Delta\tau_i$ is the optical depth of path segment i.

Numerical computation of apparent thermal path radiance for a given Cartesian location and LOS look direction is implemented by Romberg integration over two possible paths:

1. A path that starts at the observer/sensor position and terminates at the target. This path type is used to estimate the path radiance originating between the observer and target.
2. An upward-looking LOS path that starts at the target and terminates at the top of the atmosphere (TOA) or cloud base, or a downward-looking LOS path that starts at the target and terminates at the ground plane or cloud top. This upward or downward path is used to estimate the background radiance observed at the target position.

When an integration range step is reached where the optical depth of the atmospheric medium exceeds a preset limit (before the geometric terminus is reached) for either of these path types, the integration is terminated at this intermediate position.

The integrand used in the Romberg integration is the right-hand side of eq 30, also termed the "path function," specified at a discrete set of range points. The vertical profiles of extinction coefficient and air temperature are fitted with cubic splines to allow specification of extinction coefficient, optical depth, and air temperature at arbitrary ranges from the observer position.

During the range-stepped calculation of the path function integrand, if the value of the integrand at a given range point falls below a very small specified fraction of the integrand value at the start point of the path, the terminus of the path is reset to that range value and the discrete set of integrand points is recalculated. This truncation procedure ensures that the Romberg integration is performed only over the optically significant portion of the LOS path. A cubic spline fit is performed over the discrete integrand set, and is used to specify the value of the integrand at arbitrary range points in the Romberg integration routine.

4.2 Cloud/Geometrical Considerations

Natural water clouds are sufficiently dense at IR wavelengths that embedding sensors or targets within a few tens of meters within the cloud layer yields optical depths large enough to reduce the target signature below detectability. For this reason, only a single cloud layer is modeled by the IR radiance algorithm, and then only as a background for the target. Note that the geometry of the LOS is adjusted if it intersects this layer. The criteria used to adjust the LOS are illustrated schematically in four scenarios (a)–(d) in figure 3. Notionally, the sensor and target are located at the tail and head of the LOS arrows displayed in the diagram, respectively. The left arrow of each pair of arrows is the "before adjustment" arrow. The right arrow shows how the LOS appears after adjustment in each instance.

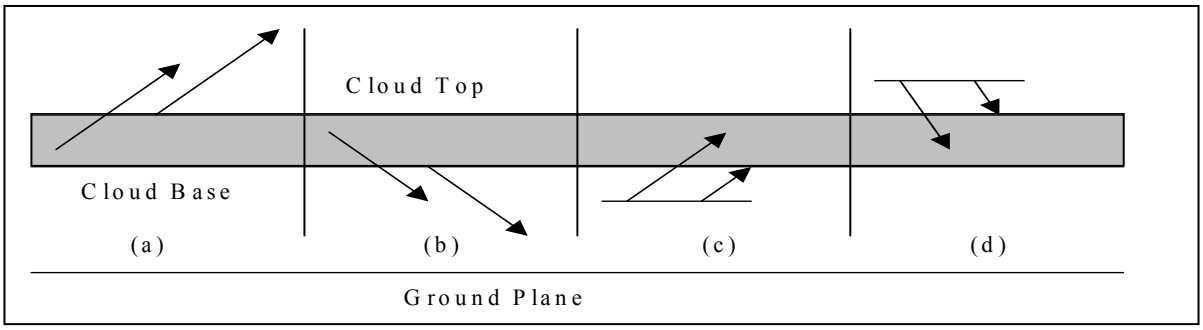

Figure 3. Diagram illustrating the criteria used to adjust the LOS when it intersects a cloud layer.

If only the observer/sensor lies within the cloud layer, the observer is relocated to a position just above the cloud layer for an upward-looking LOS—scenario (a) in figure 3. The original zenith angle of the LOS is preserved and the length of the LOS path is held constant (i.e., the target position is also moved upward by the same amount as the sensor), if possible. If the target height exceeds the nominal maximum of 5.0 km above ground level (AGL), the target altitude is set to this maximum and the LOS length is shortened to maintain the user-specified zenith angle. The downward-looking LOS of scenario (b) follows a similar adjustment procedure, with the

observer/sensor position being reset to be just below the cloud and the target height being adjusted to keep it AGL, if necessary.

If only the target is embedded within the cloud layer, as in scenarios (c) and (d), the LOS is adjusted to keep the observer position and LOS zenith angle fixed, with the target height revised so that the cloud base or top is a background behind the target.

If both the observer/sensor and target are embedded within the cloud layer and the LOS is horizontal, or upward-looking, the reset procedure of scenario (a) is used (i.e., the entire LOS path is translated so that the observer is just above the cloud top). Fully embedded downward-looking LOS paths follow the scenario (b) adjustment procedure (i.e., the LOS is translated so that the observer is just below the cloud base).

5. Validation and Verification

5.1 Visible Wavelengths

A number of runs were made at visible wavelengths for V&V purposes. As detailed below, the algorithms used in the IR band were compared with MODTRAN (*20*) 3.5 (from this point forward we will drop the MODTRAN version number).

In the visible band, comparisons were made using another delta-Eddington SGR code (*21*), referred to in table 1 as "ΔE." The quantity examined for verification purposes was the path radiance, I_p. To reduce the number of variables some input quantities were held constant—the solar zenith and azimuth were fixed at 60º and 180º, respectively; the LOS azimuth was held fixed at 0º; the aerosol type was rural; the observer height was fixed at 10 m; and clouds were not included. The results are presented in table 1. Considering the low values of the path radiance, the agreement is good.

Table 1. Comparison of SGR results at visible wavelengths.

Visibility (km)	LOS Zenith	I_p (SGR)	I_p (ΔE)	Percentage of Difference	Target Altitude (km)	Target Distance (km)
5	88.282	0.1258	0.1384	-9.1	0.31	10.004
5	88.854	0.1518	0.1377	10.2	0.21	10.004
5	89.427	0.1323	0.137	-3.4	0.11	10.004
2	88.282	0.1543	0.1432	7.8	0.31	10.004
2	88.854	0.1564	0.1422	10.0	0.21	10.004
2	89.427	0.1631	0.1413	15.4	0.11	10.004
5	89.141	0.1507	0.1374	9.7	0.31	20.002
5	45.0	0.1078	0.1066	1.1	1.01	1.4142
5	45.0	0.0703	0.0751	-6.4	0.51	0.7071
2	45.0	0.2181	0.1885	15.7	1.01	1.4142
2	45.0	0.167	0.1581	5.6	0.51	0.7071
1	45.0	0.226	0.216	4.6	0.51	0.7071

The code was also compared with the homogeneous atmosphere case presented in Lenoble (*22*), specifically Deirmendjian's (*23*) Haze L at a wavelength of 0.7 μm, with the sun directly overhead at optical depths of 0.1 and 1.0. The results, presented in figure 4, agree well with those found in Lenoble.

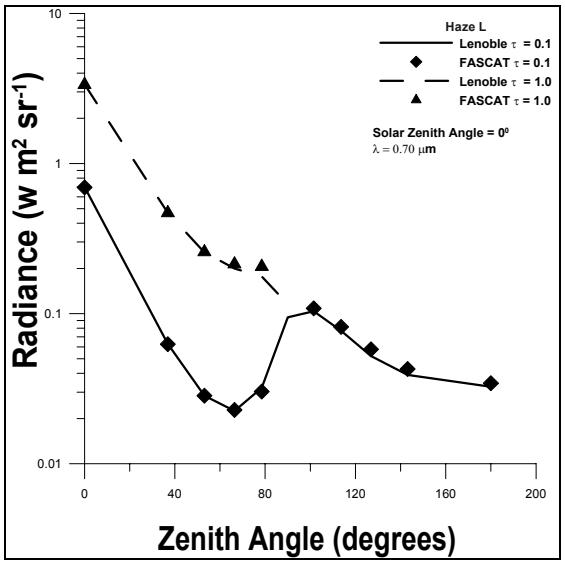

Figure 4. Comparison of results with Lenoble.

5.2 IR Wavelengths

The path and background radiances computed by the SGR model in the mid-IR (3.0–5.0 μm) and far-IR (8.0–12.0 μm) bands are assumed to be purely thermal, with no contributions from the

scattering of incident solar/lunar irradiances or the multiple scattering of thermal emission. The assumption of negligible solar scattering is of questionable validity for mid-IR band wavelengths shorter than about 4.2 μm under strong daytime illumination. (*24*) Large aerosol particles (such as rain or snow) might also violate the non-scattering assumption. Otherwise, this assumption appears to be reasonable (i.e., for wavelengths above 4.2 μm, or under subdued twilight or night lighting conditions). With these limitations in mind, the IR radiance (IRRAD) routine in the SGR model was compared with the MODTRAN atmospheric transmission/radiance model. We attempted to maintain equivalent environmental conditions between inputs for the two models, but exact equality could not be achieved (particularly with the cloud layer models).

The environmental scenario used in this comparison is one in which a sensor situated at 1 km AGL looks upward with a zenith angle of 80º. The target is located at a range of 10 km from the sensor along this LOS, which puts it at an altitude of $1.0 + 10\cos(80°) = 2.74$ km AGL. A 1-km thick altocumulus/altostratus cloud layer is placed so that the cloud base is at an altitude of 2.4 km AGL (the cloud base height used here is the MODTRAN default for the selected cloud type). The target is thus above the cloud base (a geometry similar to that depicted in fig. 3, scenario (c)), so the target altitude is reset to be 2.4 km AGL and the target range becomes 8.06 km. Figure 5 represents this scenario.

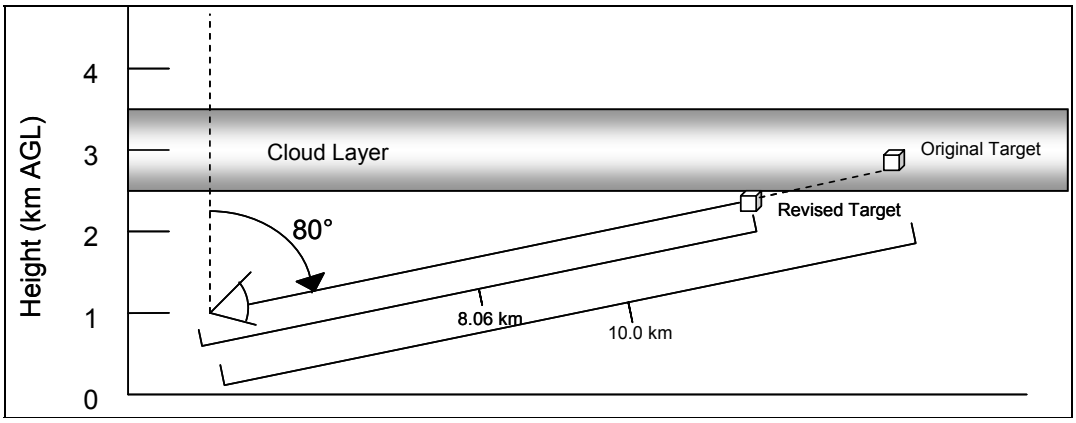

Figure 5. Scenario used for IR wavelengths showing target relocation.

Other characteristics of the comparison scenario are presented in table 2.

Table 2. Partial input parameters for IR validation runs.

Surface visibility	5 km
Haze layer aerosol type	3 (Rural)
Atmospheric model	6 (1976 U.S. Standard atmosphere)
Surface relative humidity	50 percent
Surface wind speed	0 m/s
Surface albedo	0.2
Surface (ground) temperature	288.2 K

Scenario results were generated for the 3.0–5.0 μm and 8.0–12.0 μm wavelength bands at the full MODTRAN wave-number resolution (1 cm^{-1}). Figure 6 compares the spectral radiances for the path between the observer and target and for the total (path plus cloud background) spectral radiance at the observer position in the 3.0–5.0 μm band.

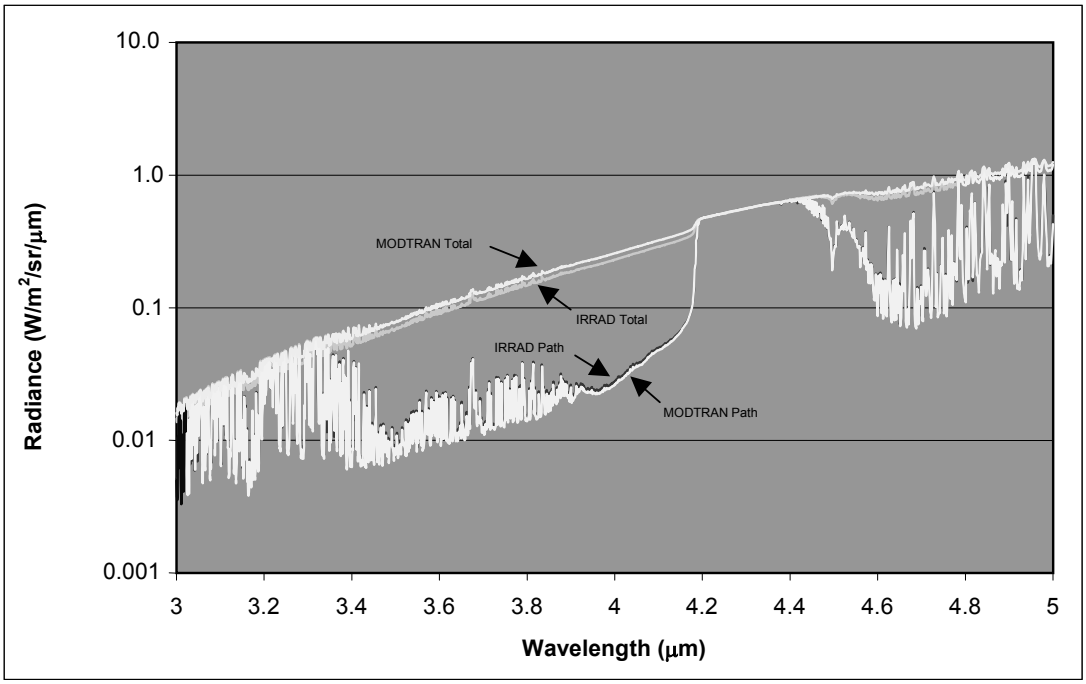

Figure 6. Comparison of MODTRAN and IRRAD spectral radiances in the mid-IR band.

The two models agree quite well for the path radiance results and reasonably well for the total radiance results. A similar comparison is made for the 8.0–12.0 μm wavelength band in Figure 7.

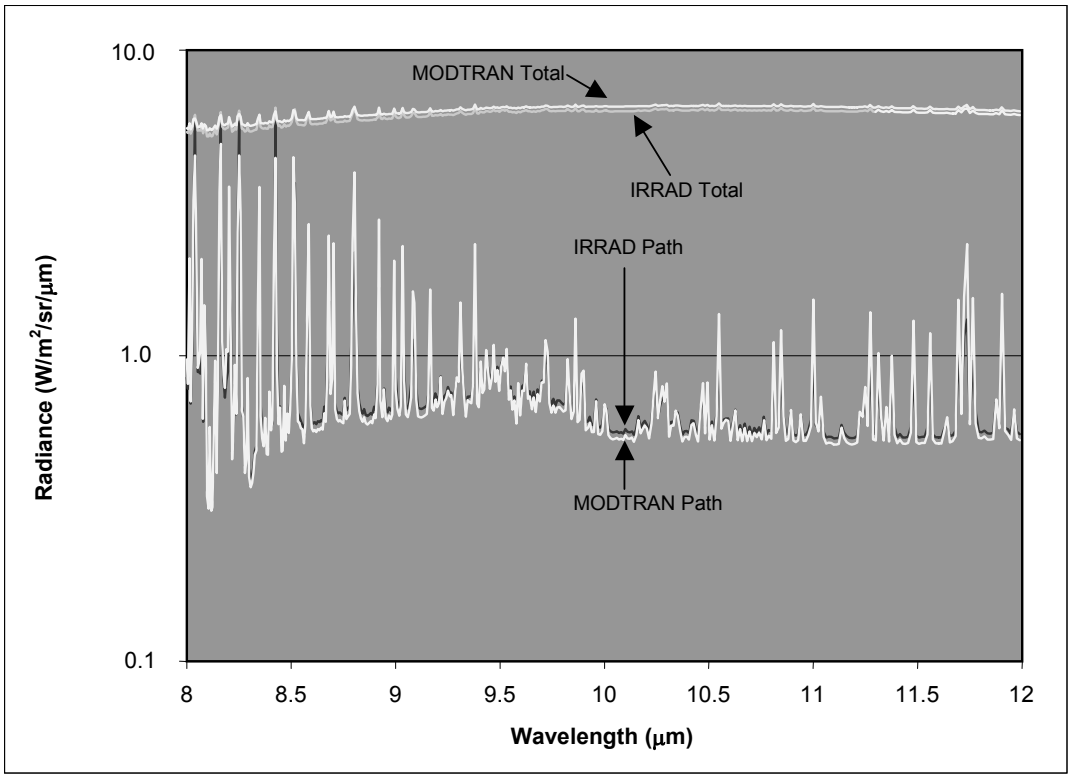

Figure 7. Far-IR spectral radiance comparison between MODTRAN and IRRAD models.

The far-IR results also show good agreement between the two models. The total radiances show better agreement in this longer band than in the mid-IR band, due in large part to the cloud layer's closer approach to blackbody behavior.

6. Usage

The program is set up to run in batch mode by piping previously scripted data from a user-supplied file. Using the batch mode minimizes errors and makes rerunning the model easier. If the user desires to have the code run in interactive mode, a slight modification to the program is necessary. Specifically, in the block data subroutine, the DATA statement for INTERACTIVE must be changed from 0 to 1; once this is done, the code will run interactively. Note that in most cases reasonable domains of validity are checked as input data are received and default values are supplied if the input datum is out of the domain range. A simple, clear-atmosphere, "canned" test case is provided to verify operation of the model on a new installation.

The program sends its results to the standard output (unit 6) in spectral form as a table and also in band-averaged or integrated form. At visible wavelengths, auxiliary output optionally goes to a log file named fasclog.out, if the parameter, iprint, located in block data, is set equal to one. If

iprint = 0 (default), fasclog.out is not created nor is output written to it. If the user has requested a run that iterates on a particular parameter, the iterated band-averaged and integrated results are written to a file named nvarfile.out.

To obtain solar/lunar geometrical information, the code makes use of the U.S. Naval Observatory's Solar-Lunar Almanac Core (SLAC), a code written in C. (*25*) SLAC is a set of integrated software modules that provides information concerning the sun and moon, which is useful for operations planning, mission scheduling, and other practical applications. Since implementation of cross-language routines is compiler specific, the user must properly interface SLAC with this program. To do this requires some type of interface between the FORTRAN and C routines, which occurs in the FORTRAN subroutines getloopvar, getvis, and setvis. The transfer of information between the FORTRAN and C code can occur by either reading/writing to a file or calling the C routine directly from FORTRAN. In either method, some set of system calls is required. In the first method, a system call would have to be made to execute SLAC as a stand-alone code. When implemented as a stand-alone code, a driver routine (Slac_optional_driver) must be included and can be found in the supplied C directory. In the second method, a system call is made to SLAC as a function; the C driver is not required. Comments are embedded in the FORTRAN routines for both methods. As supplied, the code has been interfaced on a PC using the Lahey[1] FORTRAN 90 and MICROSOFT[2] VISUAL C/C++[3] compiler mixed-language statements. Also supplied as comments are the appropriate interface statements for using the SUN[4] FORTRAN 90/C compilers. The SUN and SGI compilers are identical and, although untested on the SGI machine, it is expected that the SUN statements will work on an SGI machine. Finally, when running on a SUN machine, slac_ill.c and slac_ill.h routines need to have an underscore placed at the trailing end of the C routine names. Again, appropriate comments are included in both C routines.

In the following sections, no distinction is made between batch and interactive modes.

6.1 Inputs Common to Both Visible and IR Bands: Part 1

The program starts by requesting the wavelength band that the user would like to examine: visible (including 1.06μm), mid-IR, or far-IR (see tab. 3). It should be noted that scattering effects in the mid-IR band may be examined by choosing the visible band (*1*); however, only scattering will be considered. Emissive effects are not included when the visible band is selected.

Table 3. Choices for wavelength band selection.

Input	Value
Wavelength band selector	1 = Visible, Near-IR 2 = Mid-IR 3 = Far-IR

Subsequent to this, the program asks if the user wishes to enter an optional ASCII sensor response file. This file must reside in the same directory as the executable file, or an appropriate path must

[1] Lahey is a registered trademark of Lahey Computer Systems, Inc.

[2] Microsoft is a registered trademark of Microsoft Corp. in the U.S. and other countries.

[3] Visual C++ is a registered trademark of Microsoft Corp. in the U.S. and other countries.

[4] SUN is a trademark or registered trademark of Sun Microsystems, Inc. in the United Stated and other countries.

be provided; there is a 32-character limit on the input filename. The filename is entered in response to the question: "Will a sensor response file be used? y/n?" If the answer to this question is "y" (or "Y"), then this response function file is used to determine the wavelength band and to weight the following quantities: band-averaged SGR; transmission and contrast transmission; band-integrated path; and background radiance calculations. When such a file is present, the wavelength limits for calculating the various output quantities are taken from the sensor file, thus requiring that sensor response values to run sequentially from the smallest to largest wavelength. Once the file is read, the program renormalizes to a value of 1.0, thereby allowing arbitrary units for the response function. If the file is not present (answer is "n" or "N"), a default sensor response curve, comprised of a "flat" curve normalized to a value of 1.0, is used and the program computes the output quantities over the entire wavelength band chosen by the wavelength band selector. For the visual band, this is 0.35–0.75 μm, and for the IR band, this is 1.06 μm, 3.0–5.0 μm or 8.0–12.0 μm (note that, due to the substantial scattering effects, the near-IR laser wavelength of 1.06 μm is handled in the visual wavelength regime).

The program then asks for the surface meteorological (Met) visibility.

At this point the program branches to a specific input sequence, depending upon whether the wavelength band chosen was visible or IR. Following this wavelength band-specific input, the program requests information relevant to the observer-target geometry and iteration options. In concert with the program flow, we present the wavelength specific input followed by the common geometrical input. All inputs are concatenated and reiterated in section 6.4 (in tabs. 9 and 10) along with units, allowed ranges, and code variable names and locations.

6.2 Visible Band Model Input

The original version of this code only covered two wavelengths (0.55 and 1.06 μm) for 6 basic aerosol haze layer types. This band was extended to the following wavelength grid: 0.35, 0.40, 0.45, 0.50, 0.55, 0.60, 0.65, 0.70, 0.75, and 1.06 μm (scattering effects in the mid-IR may also be examined using the visual band selector. Note that if this is done, emissive effects are not included and the mid- or far-IR band must be selected to perform such calculations). The ARL PFNDAT92 (*26*) and PFNDAT2004 (*27*) aerosol phase function databases were used to supply all the phase function and aerosol attenuation parameters needed by the SGR program. The molecular profile of the atmosphere is fixed to be that of the 1976 U.S. Standard Atmosphere (*28*). The aerosol profile consists of a uniformly mixed haze layer of user-specified vertical depth, surface Met visibility, relative humidity, and aerosol type, surmounted by a high visibility tropospheric layer. The visibility within the boundary layer is set by the user input value and subsequently scaled exponentially from the top of the boundary layer to the model TOA, which has been set at 10.0 km. The vertical scaling of visibility above the boundary layer starts at the default value of 50 km, unless the user has input a visibility greater than 50 km in the surface haze layer, in which case that value is used as the starting point.

In the visible band, the program allows for selection of one of nineteen different aerosol types (tab. 4) for the haze layer, followed by separate requests for the thickness of the haze layer and the relative humidity of the selected aerosol.

Table 4. Choices for aerosol type at visible wavelengths and their relative humidities (percent) where applicable.

Input		Value
Aerosol Type	**Relative Humidity (%)**	**Aerosol Type Selector**
Maritime	0 50 70 80 90 95 98 99	1
Urban	0 50 70 80 90 95 98 99	2
Rural	0 50 70 80 90 95 98 99	3
Fog (heavy advection)	100	4
Fog (moderate radiation)	100	5
Rain (drizzle)	100	6
Rain (widespread)	100	7
Rain (thunderstorm	100	8
Snow	NA	9
Fog (moderate advection)	100	10
Fog (heavy radiation)	100	11
Desert aerosol[†]	NA	12
Tropospheric	0 50 70 80 90 95 98 99	13
Dust(light loading)	NA	14
Dust(heavy loading)	NA	15
High Explosive Dust	NA	16
WP smoke	17 50 90	17
Fog Oil	50	18
HC smoke	85	19

[#] The model selection is determined in conjunction with the separate relative humidity input value.

[†] Requires a wind speed of 0, 10, 20, or 30 m/s.

The code also allows the user the option of including clouds ranging from partly cloudy to totally overcast, in increments of tenths. Since the methodology for determining the probability of cloud-free line-of-sight (CFLOS) and its implementation may be found elsewhere (*13*, *29*) and because the addition of such effects does not change the basic methodology used in the code, they are not explained here. In addition to the clear-atmosphere configuration, the user may specify up to two cloud layers in the visible. It should be noted that the two-cloud layer option employs numerous assumptions (*13*) and is included as a means to obtain rough estimates of the multi-layer cloud effects on SGR. Due to limitations in the SGR program's atmospheric layering model, neither the observer nor the target should be situated within a cloud layer. Another practical constraint is that the LOS should not be interrupted by a cloud layer; otherwise, the transmission is so low that the target is invisible to the observer. This program enforces these constraints by shortening or shifting the LOS (while maintaining the LOS zenith angle) so that the LOS is in one of the clear

atmospheric zones: between the TOA and the top of the uppermost cloud layer, between cloud layers, or between the lowest cloud base and the ground. Thus, in this program cloud layers appear only as backgrounds (c.f., previous discussion in section 4.2).

Because the SGR program requires that the (up to two) user-input cloud layers do not overlap, several conditions must be observed to ensure consistent specification of the cloud layers. First, while the program currently only allows two cloud layers, there are three cloud height domains in common Met usage: high-level clouds (cirrus/cirrostratus), mid-level clouds (altostratus/ altocumulus), and low-level clouds (cumulus, stratus/stratocumulus, or nimbostratus). The SGR program's non-overlap condition requires that only one cloud type selection from each cloud height domain is used for any given visible-band run. Thus, altostratus/altocumulus and nimbostratus may be combined in a single run, but cumulus (low-level) and nimbostratus (also low-level) are not a valid combination. In the event that the first cloud layer specified is a high-level type and the second is also from the high-level domain, the program resets the second cloud layer type to be a mid-level (altostratus/altocumulus) type. The same default is used when two low-level cloud layers are specified. When two mid-level cloud layers are specified, the second layer is reset to be a high-level (cirrus/cirrostratus) type. Another impact of the non-overlap requirement is that the cloud top height for the nimbostratus low-level layer is set at 3.00 km AGL, while the base of the adjacent altostratus/altocumulus (mid-level) layer is set to 3.01 km AGL (see tab. 5). Since the user does not input explicit values for cloud top or base heights in the present version of the code, this peculiarity of the layering setup may have significance for future, though not current, implementations of the SGR model.

The program first requests the number of cloud layers, with zero indicating none; in the visible band, up to two cloud layers may be entered. The cloud type and cloud optical depth, both on the same input line, are then requested. Next, the fractional sky coverage is requested. The user should carefully note that in methodology employed in the visual portion of this code, the cloud geometrical thickness, the cloud optical depth, and the cloud fractional amount are all independent quantities. The cloud optical depth is entered as average (1), thick (2), or thin (3), with the thick and thin optical depths being one standard deviation from the average. If the user is not sure of the optical depth, this parameter may be set to zero and will default to "average." The cloud type parameter follows the cloud type numbering system in table 5. Also presented in table 5 are the altitudes of the cloud tops and cloud bases for the various cloud types. Note that for the altostratus/altocumulus (type 2) and nimbostratus (type 5) cloud types, there is a slight difference in cloud top heights between the visible and IR bands. Because of the characteristics of the polynomial fit function for extinction coefficients, which was derived from the U.S. Army EOSAEL Cloud Transmission (CLTRAN) (*30*) model, the IR cloud top heights are non-integer (i.e., floating point) values. The CLTRAN fit function uses the height above the cloud base (z) as the independent variable and starts from a positive value at $z = 0$. The function increases with z to a maximum within the cloud and then decreases until the cloud top is reached.

Table 5. Cloud types available in the program and their tops and bases.

Input	Cloud Type	Cloud Top/Base (km)	
		Visual	IR
1	Cirrus/cirrostratus	9.0/8.0	
2	Altostratus/altocumulus	5.0/3.01	4.95/3.01
3	Cumulus	2.0/1.0	
4	Stratus/stratocumulus	2.0/1.0	
5	Nimbostratus	3.0/1.0	2.98/1.0

The cloud cover (fractional sky coverage), in tenths, is entered next.

External illumination sources used in this model are limited to the sun and moon. There currently is no diffuse twilight model, so users should avoid situations where neither the sun nor the moon is above the horizon. If such a condition is specified on the initial iteration of the model, the model aborts with an error message. If the program is operated in the loop mode (see sections 6.4 and 6.5) and the "no sun or moon" condition occurs on the second or later iteration, a warning message is printed and the offending iteration cycle is skipped. Another illumination condition that should be avoided occurs when strong morning or evening twilight is present for a lunar illumination source. The program will not abort in this instance, but a warning message is output that cautions the user that the moon is competing with civil, nautical, or astronomical twilight. Two other illumination error conditions require some description. If the primary illumination source (sun or moon) is within 3º of the horizon, the delta-Eddington algorithm becomes inaccurate and/or unstable. Appropriate checks and warning messages have been implemented to exit gracefully from this condition. Another glitch occurs if the primary illumination source is the moon, and the lunar phase is close to new moon (i.e., the sun-observer-moon angle is less than 20º). Again, the appropriate checks and warnings have been implemented to avoid a software crash under such conditions.

The user may specify the solar/lunar position in the sky directly or implicitly. Under the direct method (illumination source selector = 2 or 3), the user specifies the solar/lunar zenith and azimuth angles, and phase (for the moon). The implicit method (illumination source selector = 1), which uses the SLAC model, requires the user to input the Greenwich Mean Time (GMT) time and date, as well as the observer's latitude and longitude, from which the solar/lunar zenith and azimuth angles, and phase (for the moon), are subsequently determined. Under either approach, the TOA irradiance for the specified wavelength and illumination source (sun/moon) is obtained with the help of the SOURCE routine from MODTRAN. The illumination source selector, and quantities dependent upon that selection, are presented in table 6.

Table 6. Available illumination sources in the visible.

Illumination Source Selector	Source	Required Input Data Records
1	Sun or Moon	observer latitude (degrees N)
		observer longitude (degrees E)
		scenario GMT (HH MM)
		month day year (MM DD YYYY)
2	Sun	solar zenith angle (degrees)
		solar azimuth (degrees E of N)
3	Moon	lunar zenith angle (degrees)
		lunar azimuth (degrees E of N)
		"phase" angle between the Sun and Moon as seen from Earth (in degrees: 0º = New Moon, 180º = Full Moon)

After the atmospheric and illumination input, the user must specify the LOS geometry. In all visual cases, the user enters the azimuth of the LOS. This input follows the usual Met convention (i.e., an azimuth angle of 0º implies an observer looking north and an azimuth angle of 90º implies that the observer is looking eastward). LOS geometry, ground, background information, and iteration options may be found in sections 6.4 and 6.5.

6.3 IR Band Model Input

A second model employed in this code treats the mid-IR and far-IR spectral bands. The dominant contributions to path and background radiance in these bands are usually due to greybody thermal emission, although aerosol scattering of solar irradiance and thermal emission can be dominant effects at low Met visibilities for wavelengths shorter than 4.2 μm. Thus, the IR band model implemented here ignores scattering contributions, but does require an atmospheric temperature profile, a molecular absorption profile, profiles of aerosol extinction and absorption, background temperature, and background emissivity (determined through the albedo). The background temperature and albedo are user-supplied directly; the temperature, molecular, and aerosol profiles are program-supplied via user input choices, including model atmosphere, lower atmosphere haze aerosol type, surface relative humidity (for hygroscopic aerosols), and surface wind speed (for desert aerosols).

Because the current version of the IR model is relatively limited in its description of the atmospheric environment, inputs to this model are simpler than for the visible band case. As in the visible case, the wavelength band to be covered is taken from the beginning/ending sensor response file (if supplied); otherwise the entire wavelength band is used, which in the mid-IR is 3.0–5.0 μm with a default wavelength increment of 0.1 μm, and in the far-IR is 8.0–12.0 μm with the same wavelength increment. As in the visible case, the user also specifies a surface Met visual range but, unlike the visible band case, the user does not specify the haze layer depth, illuminating source properties, or LOS azimuth angle. The IR model input also shares the following parameters with the visible band: cloud type (cloud optical depth is not required for IR runs), surface relative humidity, multimode LOS range-altitude inputs (i.e., LOS zenith angle, target range, target altitude, observer altitude), background surface albedo, and an optional elevated background range behind

the target position. The IR model additionally requests a model atmosphere profile, an additional surface haze layer aerosol type (desert), a surface wind speed (only required when the desert aerosol model is invoked), and a background surface temperature. It does not request the zenith or azimuth angle of the background surface since the surface is assumed to be a simple Lambertian greybody thermal emitter. The user may also request loop operation for the zenith angle parameter (only).

The vertical temperature and humidity profiles used in the IR portion of the program depend on the user's selection of the model atmosphere from a list of six standard AFGL model atmospheres. The air temperature for each model is specified at eight altitudes, ranging from ground level to 9 km AGL (note that this differs from the visual band case). Each model's profile for molecular absorption was obtained by running MODTRAN over a horizontal path at each model atmospheric level under the appropriate model conditions. The horizontal path length was adjusted so that the resulting spectral transmissions could accurately be transformed to yield molecular absorption coefficients. This was not a trivial task, as the strength of the molecular absorptions varies quite markedly over the IR band (it is especially pronounced in the 3.0–5.0 μm band). In practice, short and long path runs of MODTRAN had to be made at the denser, lower atmospheric levels in order to provide satisfactory profiles. MODTRAN was run at maximum spectral resolution (1 cm^{-1}) for this task in both bands (3.0–5.0 μm and 8.0–12.0 μm). It should be noted that even at the maximum MODTRAN spectral resolution, some narrow absorption features are not well represented in the results (which are stored in the mirdata.inp and firdata.inp data files). However, line wing and continuum features that are larger than the wave-number bin spacing are adequately represented by the MODTRAN band model. Because the molecular absorption coefficient generally varies quite rapidly with wavelength, this quantity is averaged at the beginning of each model run between the wavelength values that are specified by the user's sensor response file or by the default wavelength spacing. This averaging is performed before any radiative transfer calculations are undertaken and is deemed appropriate for broadband sensors encountered in IR scenarios.

Aerosol extinction and absorption coefficients for the surface haze layer are defined using the same PFNDAT database and a similar methodology to that described in the visible band section above. The aerosol haze layer is assumed to be uniform from 0 to 2 km AGL, with an extinction coefficient that is wavelength-scaled to the surface Met visibility (minus the nominal Rayleigh molecular scattering coefficient). The aerosol above the haze layer is fixed as the tropospheric type (relative humidity of 50 percent), consistent with a horizontal surface visibility of 50 km. The tropospheric aerosol profile is adjusted to be consistent with either of two aerosol density profiles (from MODTRAN) that are specific to the model atmosphere chosen by the user. This limitation is not regarded as especially significant, as the aerosol contribution to the total absorption coefficient is not dominant.

A natural cloud IR emission model was also developed and is included in the current version of this software. This model is preliminary, in the sense that some parameters necessary for the thermal radiance calculations are only roughly estimated. Various models and data sources were combined to create the cloud emission model. Vertical profiles of extinction in the two IR bands were obtained from the CLTRAN model (c.f. discussion on cloud layers in the section 6.2 "Visible Band Model Input"). Single scattering albedo estimates were obtained from Shettle and Fenn (*31*).

Cirrus cloud single scattering albedos were estimated from Web-published data from the MODIS (*32*) experiment.

The CLTRAN cloud type designations were converted to be similar to those used as inputs for the visible band model discussed above (the ICLTYPEn parameter values have the same meaning here as in the visible band case). It is important to remember, however, that the basic cloud property models derive from different sources, so that comparison of visible and IR results must be approached with caution.

Unlike the visible band case, the IR bands only permit the presence of a single cloud layer and do not require a user input optical depth. Due to the large optical thickness of these clouds in the IR, radiance results from different cloud types are very similar (with all other parameters held constant). Selection of different cloud types is allowed; however, the altitude of cloud bases and tops vary from type to type. The cloud parameters used in the program are presented in table 5. Because of the vertical variation of ambient atmospheric temperature, the resulting thermal radiances will vary as well. The cirrus cloud type is arbitrarily assumed to have a layer optical depth of unity in both IR bands. This intermediate optical depth will cause significant variation of thermal radiance with LOS zenith angle, unlike other cloud types. In addition, because of the location of the cirrus layer in the colder upper atmosphere (and its relative optical thinness), the thermal radiance results for these clouds will be lower than for the other cloud types.

Thus, the only input specific to IR wavelengths is the absence/presence of clouds and, if present, the type of cloud. The temperature of the ground surface is also required. It should be noted that the presence of a cloud layer will modify the water vapor profile (of the cloud-free atmosphere) in the vicinity of the layer. This will cause some inaccuracy for estimates of path transmission and radiance in the IR, especially in strongly-absorbing regions of the IR bands. However, the primary focus of this model is for sensors or targets that are situated substantially lower than 1 km AGL. With that proviso, the atmospheric regions that are adjacent to cloud layers appear only as backgrounds, and their radiance/transmission signatures are dominated by those of any extant cloud layers.

6.4 Inputs Common to both Visible and IR Bands: Part 2

The user specifies the LOS geometry for a given model run using one of three methods. The determination of four additional required parameters—LOS zenith angle (measured positive from the zenith downward), target range from observer, observer altitude, and target altitude—is handled by selecting one of the three modes, shown in table 7. Given any three of the LOS parameters, the fourth can be calculated. Thus, the program first asks for which LOS mode the user wishes to employ and then asks for the appropriate parameters necessary to calculate the fourth parameter. The modes, required input, and calculated value (“action”) are shown in table 7.

Table 7. Required data input for LOS mode chosen.

LOS Mode	Required Data Input Records	Action
1	LOS zenith angle (degrees)	Target altitude is calculated
	target range (km)	
	observer altitude (km)	
2	Target altitude (km)	LOS zenith angle is calculated
	target range (km)	
	observer altitude (km)	
3	LOS zenith angle (degrees)	Target range is calculated
	target altitude (km)	
	observer altitude (km)	

If cloud layers have been previously stipulated, the LOS geometry is modified if it conflicts with the CFLOS constraint mentioned above. The details of the checking/modification process are given in the comments embedded in the getcom routine.

The user then specifies the albedo of the ground surface, assumed to be Lambertian and uniform in extent. In addition, if an IR scenario has been chosen, the ground temperature is requested.

An option has been added to allow the user to specify an elevated solid background behind the target for an upward-looking, downward-looking, or horizontal LOS—e.g., when a ground-based observer views a low-flying helicopter in front of a hillside, or a ground vehicle is being observed against a hillside, tree line, etc. If this option is chosen, then the user must specify the zenith and azimuth angles of the background normal as well as the distance from the background to the target in the direction of the LOS. This option is invoked by answering "y" or "Y" to the question: "Is the background behind the target a hillside, tree line, etc.?" If the answer is "yes," then the user must specify the orientation of (zenith and azimuth angle of background normal) and distance to (from the target along the LOS) this background.

Finally, the user may choose to iterate the given scenario over one of several critical parameters. The user selects an "iteration mode" to decide which parameter to iterate over. When this option is selected, the program expects beginning values, ending values, and the number of increments between these values (see tab. 8). Note that for the IR scenarios, only iteration modes one and two are applicable, since the azimuth and time are irrelevant parameters (see section 6.3.).

Table 8. Iteration modes.

Iteration Mode	Iterated Variable
1	No iteration (fixed time or solar/lunar position and fixed LOS configuration)
2	LOS zenith angle (fixed time or solar/lunar position and fixed LOS azimuth)
3*	LOS azimuth angle (fixed time or solar/lunar position and fixed LOS zenith)
4*	Time (fixed LOS configuration)
5*	Solar/lunar azimuth angle (fixed LOS configuration)
6*	Solar/lunar zenith angle (fixed LOS configuration)

* Visible wavelengths only

6.5 Input Summary

Whether an interactive or batch run is used, tables 9 and 10 present a summary of the required and optional input quantities for visible and IR run streams, respectively. Also presented in these tables are the code variable name, location (i.e., subroutine), and units. In tables 9 and 10, if a selector or mode parameter can assume one of a contiguous enumerated list of values (in column 2), the variable/location (in column 3) is specified for only the first parameter choice (i.e., "ditto" marks are omitted).

Table 9. Required input quantities for visible runs.

Input	Value(s) & Units	Variable/Location
Wavelength band selector Visible (0.35 – 0.75, 1.06)	1	iband/sgrdriver
Sensor response file supplied?	"y" or "n" (upper case ok)	waveans/sgrdriver
Sensor response filename[$]	32 character filename (including extension). Contains up to 100 wavelength (μm) and sensor response (arbitrary units) pairs; 1 pair per input line	wavelengths(i) and wgtv(i)/sgrdriver
Surface visibility	1.0 – 300.0 km	vext/sgrdriver
Aerosol type selector		
Maritime	1	iaerosol/getvis
Urban	2	
Rural	3	
Fog (heavy advection)	4	
Fog (moderate radiation)	5	
Rain (drizzle)	6	
Rain (widespread)	7	
Rain (thunderstorm	8	
Snow	9	
Fog (moderate advection)	10	
Fog (heavy radiation)	11	
Desert aerosol[†]	12	
Tropospheric	13	
Dust(light loading)	14	
Dust(heavy loading)	15	
High Explosive Dust	16	
WP smoke	17	
Fog Oil	18	
HC smoke	19	
Haze layer thickness	0 – 2.5 km	zhaze/getvis
Relative humidity	0.0 – 99.0%	rhumid/getvis
Number of cloud layers	0, 1 or 2	ncloud/getvis

Table 9. Required input quantities for visible runs (continued).

Input	Value(s) & Units	Variable/Location
Cloud type and (optical depth)*		
Cirrus/cirrostratus (average, thin, thick)	1 (1,2,3)	icltype/getvis
Altostratus/altocumulus (average, thin, thick)	2 (1,2,3)	
Cumulus (average, thin, thick)	3 (1,2,3)	
Stratus/stratocumulus (average, thin, thick)	4 (1,2,3)	
Nimbostratus (average, thin, thick)	5 (1,2,3)	
Cloud cover*	0.0 – 1.0 (in tenths)	icltenths/getvis
Illumination source selector		
Solar/Lunar (implicit specification)	1	isrcmode/getvis
Observer Latitude	0.0 ± 90.0° (N+, S-)	glati/getvis
Observer Longitude	0.0 ± 180.0° (E+, W-)	glong/getvis
Observer Time	GMT 0 – 2359 (HHMM)	igmt/getvis
Observer Date	GMT (MM DD YYYY)	imonth iday iyear/getvis
Solar	2	isrcmode/getvis
Solar Zenith angle	0.0 – 90.0°	szen/getvis
Solar Azimuth angle	0.0 – 360.0° East of North	sazi/getvis
Lunar	3	isrcmode/getvis
Lunar Zenith angle	0.0 – 90.0°	szen/getvis
Lunar Azimuth angle	0.0 – 360.0° East of North	sazi/getvis
Phase angle (between sun and moon as seen from earth; 0.0º = New Moon, 180.0º = Full Moon)	20.1‡ – 180.0º	smangle/getvis
LOS azimuth	0.0 – 360.0º, East of North	philos/getvis
LOS specification mode		
Target height is calculated	1	losmode/getcom
LOS zenith angle	0.0 – 180.0º	thetalos/getcom
Target range	0.01 – 200.0 km	targrange/getcom
Observer height	0.0001 – 5.0 km	zobs/getcom
LOS zenith angle is calculated	2	losmode/getcom
Target height	0.0001 – 5.0 km	ztarg/getcom
Target range	0.01 – 200.0 km	targrange/getcom
Observer height	0.0001 – 5.0 km	zobs/getcom
Target range is calculated	3	losmode/getcom
LOS zenith angle	0.0 – 180.0º	thetalos/getcom
Target height	0.0001 – 5.0 km	ztarg/getcom
Observer height	0.0001 – 5.0 km	zobs/getcom
Ground surface albedo	0.0 – 1.0	salbedo/getcom
Is the background behind the target a hillside, tree line, etc.?	"y" or "n" (upper case ok)	ans/getcom

Table 9. Required input quantities for visible runs (continued).

Input	Value(s) & Units	Variable/Location
Background surface normal information**		
Zenith angle	0.0 – 180.0º	surtheta/getcom
Azimuth angle	0.0 – 360.0º	surphi/getcom
Range along LOS to background	0.01 – 300.0 km	surrange/getcom
Iteration mode		
None (single iteration mode)	1	irunmode/getrunmode
LOS zenith angle mode	2	irunmode/getrunmode
Minimum zenith angle	0º	thetamin/getrumode
Maximum zenith angle	180º	thetamax/getrunmode
Number of grid points	unlimited	ncycles/getrunmode
LOS azimuth angle mode	3	irunmode/getrunmode
Minimum azimuth angle	0º	phimin/getrunmode
Maximum azimuth angle	360º	phimax/getrunmode
Number of grid points	unlimited	ncycles/getrunmode
GMT Time mode	4	irunmode/getrunmode
Minimum time	0000 – 2359 (HHMM)	igmtmin/getrunmode
Maximum time	Minimum time + 1 minute to Minimum time + 24 H – 1 minute (HHMM)	igmtmax/getrunmode
Number of grid points	2 ≤ ncycles ≤ 1440 (integer minutes)	ncycles/getrunmode
Solar/lunar azimuth angle mode	5	irunmode/getrunmode
Minimum solar azimuth angle	0º	sazimin/getrunmode
Maximum solar azimuth angle	360º	sazimax/getrunmode
Number of grid points	unlimited	ncycles/getrunmode
Solar/lunar zenith angle mode	6	irunmode/getrunmode
Minimum solar zenith angle	0º	szenmin/getrunmode
Maximum solar zenith angle	90º	szenmax/getrunmode
Number of grid points	unlimited	ncycles/getrunmode

[$] Only required with user-supplied sensor response file ("y").

* When number of clouds > 0, optical depth will default to "average" if set to 0.

[†] Requires a wind speed of 0, 10, 20, or 30 m/s.

[‡] Code limitation

** Only required when the background behind the target is some distance from the target ("y").

Table 10. Required input quantities for IR runs.

Input	Value(s)	Variable/Location
Wavelength band selector		
Mid-IR (3.0 – 5.0)	2	iband/sgrdriver
Far-IR (8.0 – 12.0)	3	
Sensor response file supplied?	"y" or "n" (upper case ok)	waveans/sgrdriver
Sensor response file name[$]	32 character file name (including extension). Contains up to 100 wavelength (μm) and sensor response (arbitrary units) pairs per input line	wvlv(i) & wgtv(i)/sgrdriver
Surface visibility	1.0 – 300.0 km	vext/sgrdriver
Cloud condition		
Clear (no clouds)	0	icltype1/getir
Cirrus/cirrostratus	1	
Altostratus/altocumulus	2	
Cumulus	3	
Stratus/stratocumulus	4	
Nimbostratus	5	
Model Atmosphere		
Tropical	1	model/getir
Midlatitude Summer (45N, July)	2	
Midlatitude Winter (45N, Jan.)	3	
Subarctic Summer (60N, July)	4	
Subarctic Winter (60N, Jan.)	5	
1976 US Standard Atmosphere	6	

Table 10. Required input quantities for IR runs (continued).

Input	Value(s)	Variable/Location
Haze Aerosol Type		
Maritime	1	iaerosol/getir
Urban	2	
Rural	3	
Fog (heavy advection)	4	
Fog (moderate radiation)	5	
Rain (drizzle)	6	
Rain (widespread)	7	
Rain (thunderstorm)	8	
Snow	9	
Fog (moderate advection)	10	
Fog (heavy radiation)	11	
Desert aerosol†	12	
Tropospheric	13	
Dust(light loading)	14	
Dust(heavy loading)	15	
High Explosive Dust	16	
WP smoke	17	
Fog Oil	18	
HC smoke	19	
Surface Wind Speed†	0 – 30 m/s	surfwind/getir
Surface Relative Humidity	0.0 – 99.0 percent	surfrh/getir
LOS specification mode		
Target height is calculated	1	losmode/getcom
LOS zenith angle	0.0 – 180.0º	thetalos/getcom
Target range	0.01 – 200.0 km	targrange/getcom
Observer height	0.0001 – 5.0 km	zobs/getcom
LOS zenith angle is calculated	2	losmode/getcom
Target height	0.0001 – 5.0 km	ztarg/getcom
Target range	0.01 – 200.0 km	targrange/getcom
Observer height	0.0001 – 5.0 km	zobs/getcom

Table 10. Required input quantities for IR runs (continued).

Input	Value(s)	Variable/Location
Target range is calculated	3	losmode/getcom
LOS zenith angle	0.0 – 180.0º	thetalos/getcom
Target height	0.0001 – 5.0 km	ztarg/getcom
Observer height	0.0001 – 5.0 km	zobs/getcom
Ground surface albedo	0.0 – 1.0	salbedo/getcom
Ground surface temperature	0.1 – 1000.0 K	tgrnd/getcom
Is the background behind the target a hillside, tree line, etc.?	"y" or "n" (upper case ok)	ans/getcom
Background surface normal information**		
Zenith angle	0.0 – 180.0º	surtheta/getcom
Azimuth angle	0.0 – 360.0º	surphi/getcom
Range along LOS to background	0.01 – 300.0 km	surrange/getcom
Iteration mode		
None (single iteration mode)	1	irunmode/getrunmode
LOS zenith angle	2	
Minimum zenith angle	0º	thetamin/getrumode
Maximum zenith angle	90º	thetamax/getrunmode
Number of grid points	unlimited	ncycles/getrunmode

[$] Only required with user-supplied sensor response file ("y").

[†] Only required with desert aerosol model (aerosol type 12).

**Only required when the background behind the target is some distance from the target ("y").

7. Output

The program begins by printing out some informative text concerning the geometry and wavelength selected. It then prints out the user-selected input quantities followed by the spectral and band-averaged/band-integrated values (listed in table 11) at the actual wavelengths used. The numerical procedures used to generate band-averaged and band-integrated results for a spectral quantity A are as follows:

$$\overline{A} = \frac{\sum_{i=1}^{N} A_i w_i}{\sum_{i=1}^{N} w_i} \quad \text{(band-averaged)}, \tag{28}$$

and

$$A_{\text{int}} = \sum_{i=2}^{N} \frac{A_i w_i + A_{i-1} w_{i-1}}{2} \; (\lambda_i - \lambda_{i-1}) \quad \text{(band-integrated)}, \tag{29}$$

where w_i are the sensor response values and A_i are the parameter values specified on the discrete wavelength grid λ_i. The sensor response values are normalized to the maximum sensor response, i.e., w_i is always less than unity, with a uniform response sensor showing unity response over the band.

Table 11. Output.

Spectral Parameters
Sensor response function SGR Contrast transmission Transmission Path radiance Background radiance
Band-averaged*/Integrated# Parameters
SGR* Contrast transmission* Transmission* Path radiance* (W m^{-2} sr^{-1} μm^{-1}) Background radiance* (W m^{-2} sr^{-1} μm^{-1}) Path radiance# (W m^{-2} sr^{-1}), Background radiance# (W m^{-2} sr^{-1})

When runs are iterated over a specific parameter the output is presented on the screen and the band-averaged and band-integrated values as a function of the iterated variable are stored in the file nvarfile.out.

8. Ancillary Data Files

There are a number of ancillary data files that the program uses to read input, provide necessary data and to hold output from iterated runs. These files are presented in table 12. The aerosol information files (supplied), which contain the extinction coefficients, phase functions, etc., must be in a subdirectory named pfndat located in the directory from which execution is occurring.

Table 12. Ancillary file information.

Data Filename	Subroutine Opened In	Purpose/Contents	Read Only?
user-supplied sensor file†	sgrdriver	*Optional* file containing sensor response curve	Y
sunbd.inp	sunbd	Solar irradiances [w cm^{-2} / cm^{-1}] tabulated at wave numbers from 0 to 50,000 cm^{-1} at 5 cm^{-1} spectral resolution	Y
pfndat (directory)	phazef	Aerosol extinction & absorption coefficients, asymmetry factors and phase functions for each relative humidity, wavelength and angle (where applicable)	Y
mirdata.inp	data_initialization	Wavelength (3.0-5.0 μm), molecular and extinction coefficients as a function of altitude	Y
firdata.inp	data_initialization	Wavelength (8.0-12.0 μm), molecular and extinction coefficients as a function of altitude	Y
fasclog.out*	gendeck	Output file; provides ancillary information	N
nvarfile.out	sgrdriver	Iterated run output (see 'Common Input 2' above)	N
slac_illum.inp	getloopvar, getvis, setvis	*Optional* input file when running SLAC from a command line interface in stand-alone mode	N
slac_illum.out	getloopvar, getvis, setvis	*Optional* output file for running SLAC from a command line interface in stand-alone mode	N

* Visible wavelengths only: requires parameter iprint be set equal to 1 in block data.

† Example files are provided, e.g. visible_input.txt, mid-ir_input.txt, far-ir_input.txt.

9. Example Runs

9.1 Visible Band Examples: Scenario Construction

The following scenario simulates an airborne target moving in a horizontal line at 100.1 meter altitude across an inclined LOS under cloudless skies at visible wavelengths. A uniform sensor response file was used. The azimuthal view of this scenario is shown in figure 8; the zenith view is shown in figure 9. Other relevant parameters are presented in table 13. Note that in the nomenclature used here, LOS zenith angles ≥ 0 and < 90º[5] imply an upward looking path; LOS zenith angles > 90º[5] and ≤ 180º imply a downward looking path. Similarly LOS azimuth angles > 0º and < 180º imply the sun (or source) is in front of the observer; LOS azimuth angles > 180º and < 360º imply the sun is behind the observer. Table 14 presents a sample input script file for one of the upward looking runs: column 1 contains the required parameter, column 2 presents an identifier for user ease; the program only reads information in the first column. This input file has a LOS azimuth of 90º and zenith angle of 70º—note that the program will compute the target's distance; all LOS zenith and azimuth angles used for figures 10–13 may be found in table 13. Results from this particular run may be found in the appendix for comparison purposes; the input file is supplied with the source code as visible_input.txt.

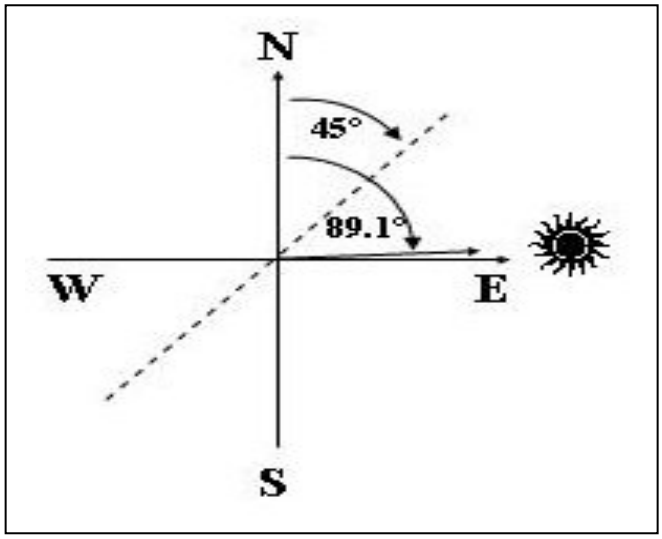

Figure 8. Top-down (azimuthal) view of scenario.

[5] Codes, such as FASCAT, that use plane-parallel geometry do not admit to a solution for horizontal paths.

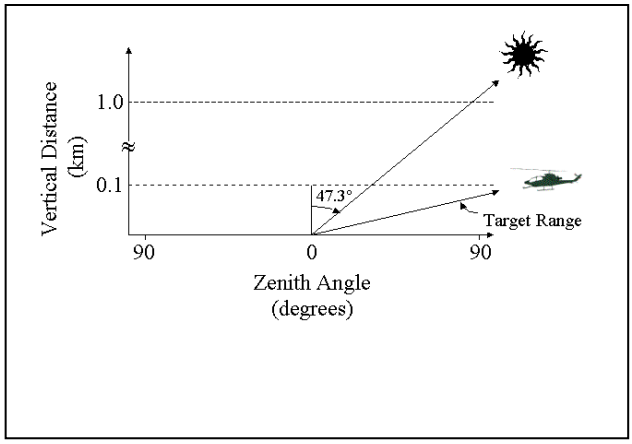

Figure 9. Horizontal (zenith) view of scenario.

Table 13. Upward and downward looking scenarios for LOS azimuth of 90° and 270°.

Time/Date/Location			**Weather**	
Time 0800 local	*Date* 1 June 2002	*Location* Latitude 32.5° Longitude 127′0″ E	*Aerosol* Urban at 90-percent relative humidity, 1-km thick	
Solar Zenith Angle 47.3º	*Solar Azimuth Angle* 89.1º		*Visibility* 2 km	*Surface Albedo* 0.2
Upward LOS			**Downward LOS**	
LOS Azimuth 90º* and 270º	*Target height:* 100.1 m *Observer height:* .1 m		*LOS Azimuth* 90º and 270º	*Target height:* 0.1 m *Observer height:* 100.1 m
Zenith Angles (degrees) 0 10 20 30 40 50 60 70* 80 89			*Zenith Angles (degrees)* 91 100 110 120 130 140 150 160 170 180	

* Appendix run.

Table 14. Script file for example scenario.

1	waveband selector
n	sensor response file?
2.0	surface visibility
2	aerosol type
1.0	haze layer depth
90.0	relative humidity
0	# of cloud layers
1	illumination selector
32.5	latitude
127.00	longitude
0000	Greenwich mean time
06 01 2002	month day year
90.	los azimuth angle
3	los mode
70.	los zenith angle
.1001	target height
.0001	observer height
0.2	surface albedo
n	target silhouetted?
1	iteration mode

9.1.1 Example 1: SGR, Radiance and Transmission as a Function of Observer Look Angle at a Fixed Wavelength

For upward looking runs the SGR, the transmission, path radiance and background radiance for LOS azimuth pairs of 0º and 180º, 45º and 225º, and 90º and 270º are presented in figures 10 through 12. For a downward looking path, results are presented for LOS azimuth pairs of only 90º and 270º in figure 13. The upward-looking scenarios simulate a helicopter flying at a constant altitude, approaching the observer from the solar direction, flying over the observer's head, and proceeding directly away from (behind) the observer with the sun now at the observer's back. The downward-looking scenario is identical, with the exception that the observer's and helicopter's positions have been interchanged. For upward-looking scenarios, we first set the azimuth such that the observer was oriented towards the sun, and then varied the LOS zenith angle from 0º to 89º. We then reoriented the observer by adding 180º to the azimuth, resulting in the sun being behind the observer, and once again varied the LOS zenith angle from 0º to 89º. For the downward-looking scenario, the observer and target positions were interchanged, the LOS azimuth was varied by 180º and the LOS zenith angle varied between 91º and 180º.

We first examine the upward looking scenarios (figures 10–12). In all figures the transmission is well behaved, being a maximum at the minimum LOS zenith angle of 0º and a minimum at the maximum LOS zenith angle of 90º. The SGR is well behaved, being less than 1, determined primarily by the strong background radiance looking upward through a relatively clear atmosphere. The double dip in the background radiance in figure 12 that occurs at 22.3º and 72.3º is due to the

delta approximation cutoff angle (θ_o) being set to 25º (see subroutine tanit). Thus, for the solar zenith angle used in this example (47.3º), the change in the phase function from peaked to truncated occurs exactly at those angles. The background radiance in the solar direction has also been truncated where it exceeds the scale. Although not so pronounced, the change in the path radiance in this figure occurs for the same reason. The plane-parallel technique used also becomes increasingly inaccurate with LOS zenith angles within ± 15º of the horizontal direction. These effects can easily be seen in the plots of background radiance and in the path radiance. For upward looking paths, particularly near the solar direction, it is seen that the forward scattering by aerosol particles increases both the path and background radiances, with the background radiance receiving most of this scattering due its longer path length. Recalling that the SGR is defined by $I_p/([\, I_b\, (\, 1 - T\,)\,]$, we can see that as the transmission approaches 0 (horizontal or very long slant paths), the SGR approaches 1. This is verification that, as we go to very long paths, the path radiance should approach the background radiance and the SGR should approach 1. Also, note that in figure 10 all of the curves are quite symmetrical. This is an expected result since the date (1 June) was chosen to be near the solar equinox where the sun's azimuth angle is very nearly 90º in the coordinate system being used. Thus, when looking at right angles to the solar direction, i.e., looking either north (LOS azimuth 0º) or south (LOS azimuth 180º), we expect to obtain almost identical results due to the symmetry with respect to the solar azimuth. Other geometries (figs. 11–13) do not have such a symmetrical representation.

For the downward looking path, figure 13 (note the change in the scale of the ordinate axis), we immediately see that the background radiance is, for all practicable purposes, a constant. This is expected, since most of the background radiance is determined by the solar radiation being reflected by the ground surface, and neither solar angle nor ground albedo are varied in this scenario. It is also of interest to note that the SGR, in this downward looking scenario, is greater than 1.

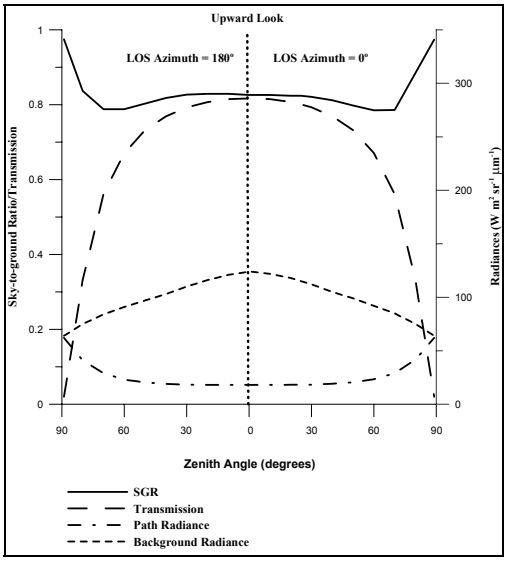

Figure 10. Upward look at right angles to solar azimuth.

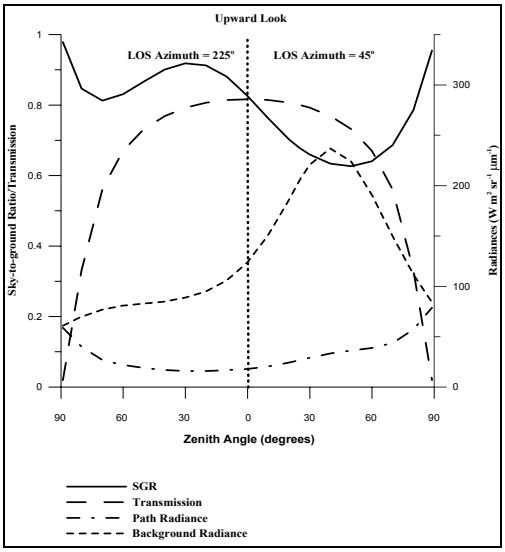

Figure 11. Upward look offset by 45° to solar azimuth.

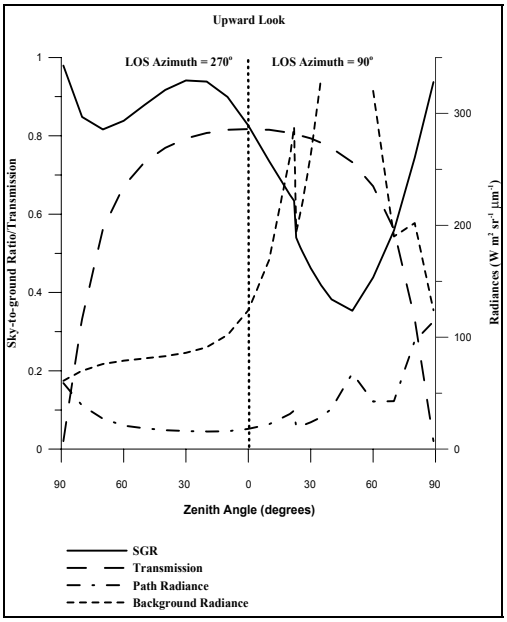

Figure 12. Upward look directly facing/behind the sun.

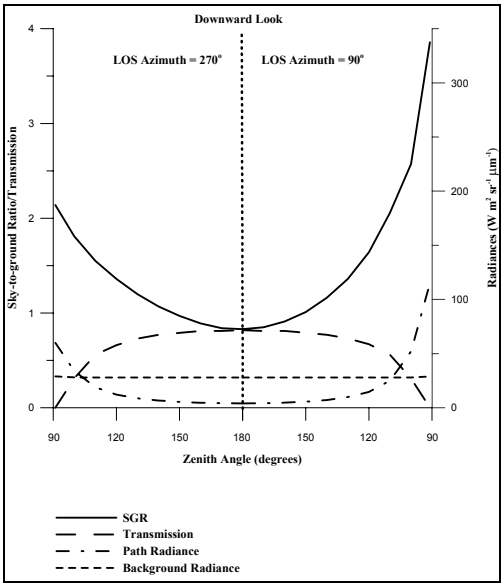

Figure 13. Downward look directly facing/behind the sun.

9.1.2 Example 2: SGR and Radiance as a Function of Range at a Fixed Wavelength

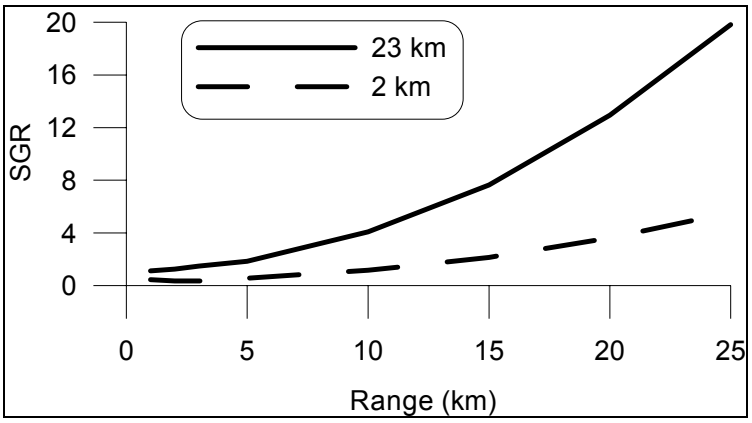

Figure 14. SGR as a function of target range at a wavelength of 0.55 μm for visibilities of 23 and 2 km.

For this example, we have used the previous scenario but, instead of examining the radiances as a function of viewing angle, we will look at them as a function of target distance, for a fixed observer height (0.0001 km), a fixed zenith angle (70º), and a surface visibility of 23 km. The SGR as a function of target range and two different visibilities along the inclined path is shown in figure 14. The figure plainly shows the variation of SGR with target range.

Figure 15 shows the various radiative components, i.e. path radiance at range r, $I_p(r)$, background radiance at distance r, $I_b(r)$; background radiance at the target distance, $I_b(0)$; and the equilibrium path radiance, I_{ps}. These components were used to calculate the SGR shown in figure 12. The apparent background radiance, $I_b(r)$, for an upward path should be constant with respect to range along that path. The values of $I_b(r)$ go from a low of 501 to a high of 513 w/m^2/sr/μm, which is within 5 percent of being constant. $I_b(0)$ dwindles with increasing range/altitude since the path length for $I_b(0)$ is approaching 0 (we are reaching the top of the atmosphere), coupled with the fact that there are fewer particles to scatter at that altitude. Eq 11 suggests that the limiting path radiance, $I_{ps}=I_p/(1-T)$ is constant for a given slant path. However, as previously mentioned, one of the problems with SGR, which was "developed" for long horizontal paths, is that if we extend this concept to slant paths we find that as one goes upward in the atmosphere the number of particulates decreases. This violates the concept of an homogeneous atmosphere, which is one of the underpinnings in the original development of SGR. So, if eq 11 is correct, why is the path radiance, I_p, asymptoting to $I_b(r)$ and not I_{ps}? Recall that $I_b(r)$ is the path radiance over the entire path under consideration (from observer to space) and I_p is the path radiance between observer and target. Since the visibility is high (23 km), I_p never approaches the equilibrium value of I_{ps}; however, as the path length between the observer and target increases, effectively moving the target towards space, I_p will approach $I_b(r)$. The problem lies in the high visibility, which leads to equilibrium values not being reached.

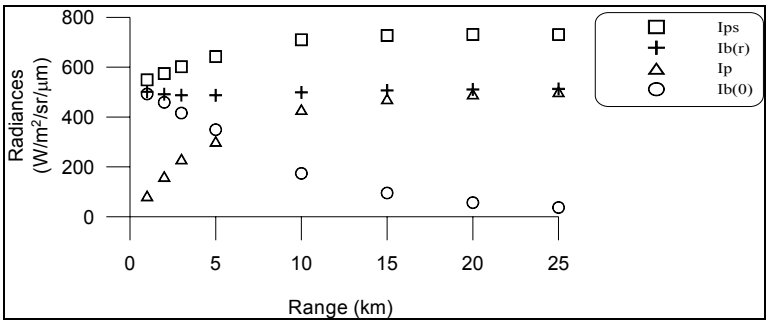

Figure 15. Component radiances vs. range. The visibility is 23 km.

Also, when using SGR one must remember the assumption that the basic underpinning of SGR is "an atmosphere homogeneous in the distribution of particulates and in illumination." Thus, we might ask, does the 70º zenith angle slant path violate this assumption? The zenith angle per se does not violate the assumption; whereas, both high visibility conditions (implying low aerosol content) and the fact that we do not have a homogeneous atmosphere along slant paths do. The underlying principle in the code is homogeneous layers. Also, note that $I_b(0)$ decreasing with range is simply due to its decreasing path length (target to space), coupled with decreasing aerosol content as we go upward in the atmosphere, not because of non-homogeneous illumination at differing altitudes.

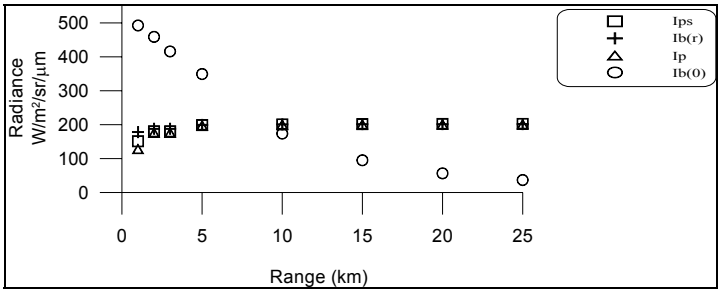

Figure 16. Component radiances vs. range. The visibility is 2 km.

Let us contrast the following figure 16, which has the same input parameters with the exception of visibility being changed to 2 km, with that of figure 15. The background radiance is still approaching zero, as expected; however, now, with the decreased visibility (or increased aerosol content) the path radiance I_p is approaching its equilibrium value I_{ps}. In addition, both of these values—I_p and I_{ps}—are now approaching the total path radiance $I_b(r)$.

9.2 IR Band Examples

9.2.1 Example 1: SGR, Radiance, and Transmission as a Function of Wavelength and Zenith Angle

The text outputs for two IR band examples are presented in the appendix. The first is a mid-IR run using the input file mid-ir_input.txt and the second is a far-IR run using the input file far-ir_input.txt. The scenario environment for these examples is essentially the same as for the visible band case listed in Table 14. Input for a representative run is presented in Table 15. Note that both of these runs require the optional sensor response file. These are provided as mir_sensor.dat and fir_sensor.dat for the mid-IR and far-IR runs, respectively. Figures 17 and 18 show the sky-to-ground ratio results for the mid-IR and far-IR results. The component

transmissions and radiances for the two bands are shown in figures 19 and 20, for a zenith angle of 70º. Note that the wavelengths at which calculations were performed for figures 17–20 were determined by the wavelength values in the user input sensor response file.

Table 15. Mid-IR band inputs for the SGR model example.

2	waveband selector
y	sensor response file?
mir_sensor.dat	input sensor response file
2.0	surface visibility
0	cloud condition
6	atmospheric model
2	haze aerosol model
90.0	surface relative humidity
1	los mode
70.0	los zenith angle
0.2924	target range
0.0001	observer height
0.2	surface albedo
273.0	surface temperature (K)
n	target silhouetted?
1	iteration mode

Table 16. Far-IR band inputs for the SGR model example.

3	waveband selector
y	sensor response file?
fir_sensor.dat	input sensor response file
2.0	surface visibility
0	cloud condition
6	atmospheric model
2	haze aerosol model
90.0	surface relative humidity
1	los mode
70.0	los zenith angle
0.2924	target range
0.0001	observer height
0.2	surface albedo
273.0	surface temperature (K)
n	target silhouetted?
1	iteration mode

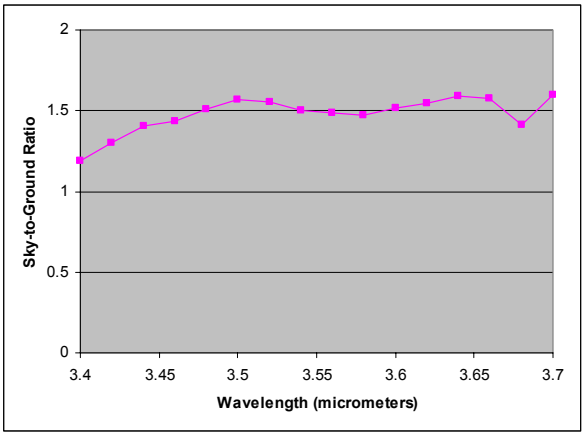

Figure 17. Mid-IR band example results: sky-to-ground ratio.

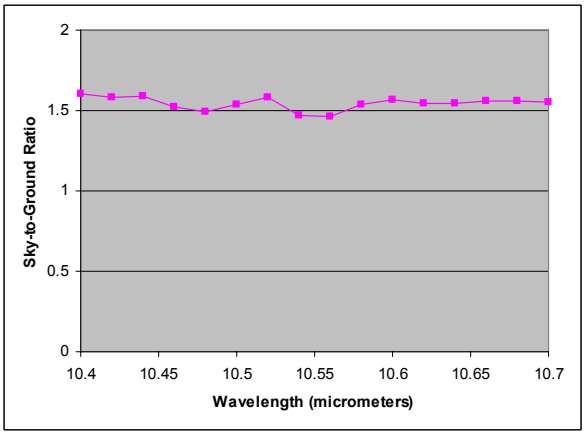

Figure 18. Far-IR band example run results: sky-to-ground ratio.

Due to the relatively short path and moderate IR visibility, most of the transmission and spectral radiance data show only slight variation over both the mid-IR and far-IR wavelength bands. The

notable exception is the background radiance at the target seen in the mid-IR results plot of figure 19. The increasingly strong molecular absorption beyond about 3.5 μm yields a strong thermal radiance background. The limiting path radiance also trends upward with wavelength due to the decreasing transmission of the LOS path, leading to a sky-to-ground ratio that varies only mildly with wavelength.

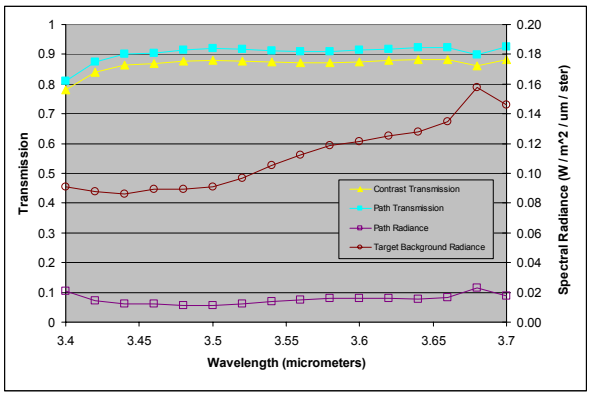

Figure 19. Mid-IR band example run results: transmission and spectral radiance

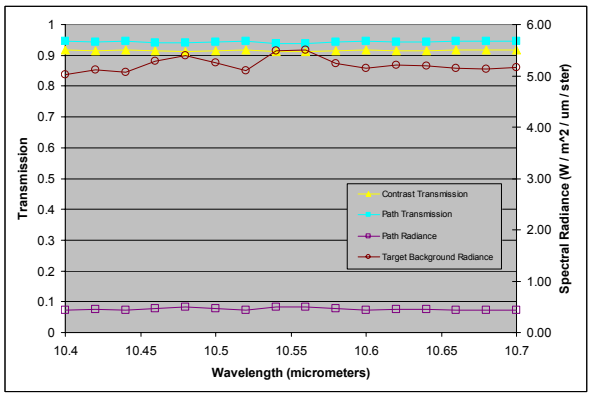

Figure 20. Far-IR band example run results: transmission and spectral radiance.

Figure 21 depicts the SGR run results for the above scenario for an upward-looking path. The target height above the near-surface observer is held constant at 0.1 km, so the LOS path length increases markedly as the zenith angle approaches horizontal (i.e., 90º). The sky-to-ground ratio shown in figure 21 decreases smoothly from its maximum at the zenith to the limiting value of unity at the horizon. The enhanced limiting path radiance at the longer (10 μm wavelength) causes the larger SGR at zenith angles that are well above horizontal.

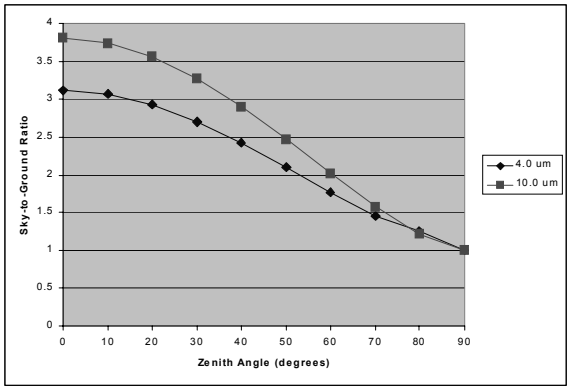

Figure 21. Sky-to-ground ratio for mid-IR and far-IR scenarios with fixed observer and target heights.

9.2.2 Example 2: SGR and Radiance as Functions of Range at a Fixed Zenith Angle

As in the visible case, the basic scenario for the IR cases was modified in this second example so that the surface visibility was much higher—23 km. The zenith angle was held constant at 70º and the observer/sensor position was held at the near-surface position (0.0001 km AGL). The target range was adjusted along the fixed LOS direction from 0.1 to 26 km. This latter range value placed the target just 0.1 km below the top-of-atmosphere boundary (9.00 km AGL) used in the SGR model. The results are shown in Figure 22 for wavelengths of 4 and 10 μm.

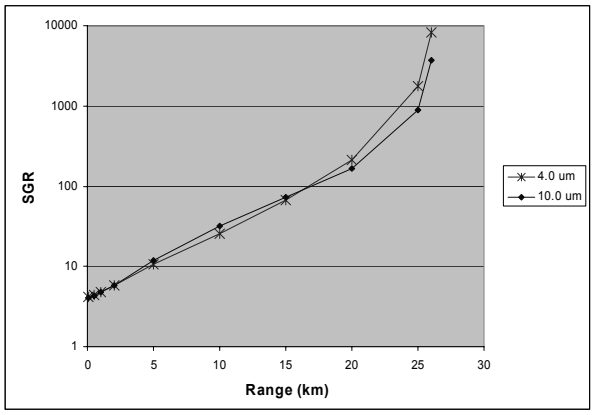

Figure 22. Sky-to-ground ratio for target range variation along a fixed zenith angle.

Figure 22 shows that sky-to-ground ratios for the 10 μm wavelength exceed those for the shorter wavelength for slant target ranges out to about 15 km (or a target altitude of about 5 km). At longer ranges or higher altitudes, the SGR rises rapidly as the amount of thermally emitting atmosphere behind the target and below the nominal top-of-atmosphere (that is the background radiance in the denominator of eq 11) begins to diminish. The background radiance at the target position for the 4 μm wavelength rolls off faster with increasing range than it does for the 10 μm case. Thus, the SGR approaches infinity as the target nears the model's TOA. For reasons of accuracy, it is best to keep the target below the uppermost atmospheric layer (i.e., below 7 km for the present code implementation).

Figures 23 and 24 display how the component radiances behave as functions of target range for the 4 and 10 μm wavelengths, respectively. As can be seen in the figures, the average limiting path radiance I_{ps} varies slowly over the entire span of target ranges. The observed path radiance I_p ramps up rapidly as the target range increases through the first 5 km and then begins to level off toward an asymptote that is well below the average limiting path radiance. As mentioned above, the background radiance at the target position $I_b(0)$ falls off very rapidly as the target approaches the nominal top of the atmosphere.

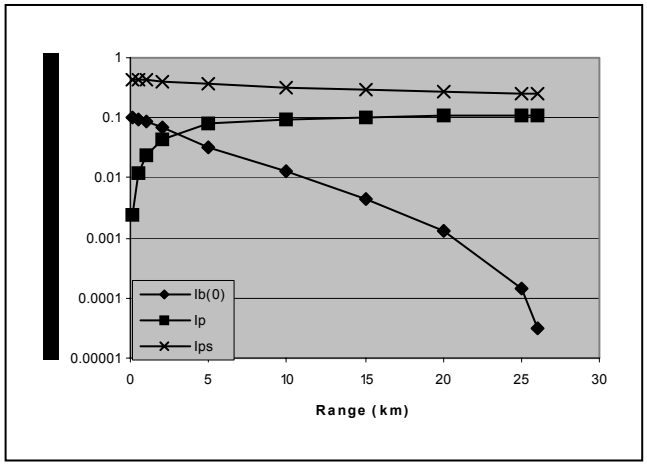

Figure 23. Spectral background, path, and limiting path radiance results for varying target ranges at a wavelength of 4 μm.

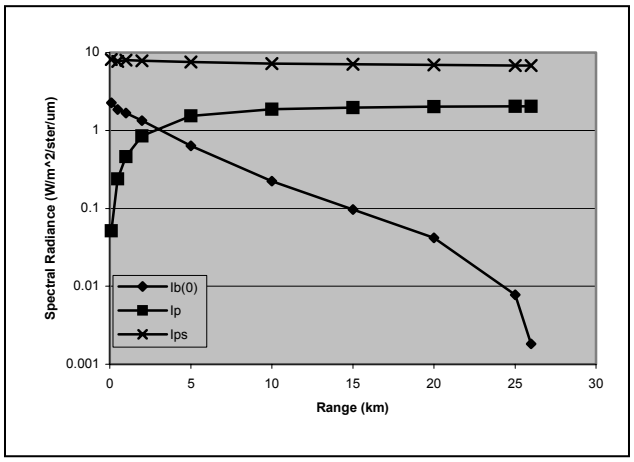

Figure 24. Spectral background, path, and limiting path radiance results for varying target ranges at a wavelength of 10 μm.

10. Caveats

The following is a summation of caveats that should be observed when using the program.

The program's wavelength maximum in the visible band is limited to 0.75μm—this is only due to the lack of appropriate phase functions. The user may run their favorite Mie scattering code, formatted as found in reference (*22*), to calculate the appropriate phase function for use at these extended wavelengths.

In the 3.0–5.0 mid-IR waveband, it should be carefully noted that scattering effects are not included.

The program is suitable only for near-earth altitudes (< 7 km).

It should be noted that even at the maximum MODTRAN spectral resolution, some narrow absorption features are not well represented in the results (which are stored in the mirdata.inp and firdata.inp data files).

It should be noted that the presence of a cloud layer will modify the water vapor profile (of the cloud-free atmosphere) in the vicinity of the layer.

The method of calculating visible radiances is approximate.

The average and the variability of cloud optical depth as a function of cloud type were determined empirically from the SOLMET (*33*) data base. The model algorithms return the optical depth for the specified cloud type and relative optical thickness (average, thick, or thin) from the table without direct reference to the specified base and top altitude of the layer. In other words, the optical thickness is determined independently of the specified geometric thickness of the cloud.

The basic cloud property models for the visual and IR derive from different sources. Therefore, comparison of visible and IR band results must be approached with caution.

11. Conclusions

We have presented a methodology for determination of the sky-to-ground ratio, complete with derivations. The program uses the delta-Eddington method for visible wavelengths and simple approximations for IR wavelengths. For ease of use, the extensive atmospheric inputs necessary to obtain realistic results have been highly automated. V&V has been carried out, delineating areas where the code's approximations break down, and user input and output have been discussed for illustrative sample scenarios/examples.

References

1. Duntley, S. Q. The Reduction of Apparent Contrast by the Atmosphere. *JOSA* **1948,** *38*, 179–191.
2. Middleton, W. E. K. *Vision through the Atmosphere;* University of Toronto Press: Toronto, Canada, 1952.
3. Evans, K. F. The Spherical Harmonic Discrete Ordinate Method for Three-dimensional Atmospheric Radiative Transfer. *J. Atmos. Sci.* February **1998**, *55*, 429–446.
4. Wetmore, A. E.; Zardecki, A. The Boundary Layer Illumination and Radiative Balance Model (BLIRB). *Proceedings of the Cloud Impacts on DOD Operations and Systems 1993 Conference, PL-TR-94-2188,* Ft. Belvoir, VA, 1993; pp 201–206.
5. O'Brien, S. G.; Tofsted, D. H. Physics-based Visualization of Dense Natural Clouds. II: Cloud-rendering Algorithm. *Appl. Opt.* November **1998**, *37*, 7680–7688.
6. Tofsted, D. H.; O'Brien, S. G. Physics-based Visualization of Dense Natural Clouds. I: Three-dimensional Discrete Ordinates Radiative Transfer. *Appl. Opt.* November **1998**, *37*, 7718–7728.
7. Dixon, D. TRAC-WSMR. Private communication, 2004.
8. Hoock, D. W.; Sutherland, R. A. Obscuration Countermeasures. In *The Infrared and Electro-Optical Systems Handbook*, vol. 7; Dudzik, M. C., Ed.; Infrared Information Analysis Center and SPIE Optical Engineering Press, 1993.
9. Miller, A. *FASCAT Atmospheric Illumination Module*, users guide; ASL-TR-0221-22; October 1987.
10. Shettle, E. P.; Weinman, J. A. The Transfer of Solar Irradiance Through Inhomogeneous Turbid Atmospheres Evaluated by Eddington's Approximation. *JAS* October **1970**, *27*, 1048.
11. Joseph, J. H.; Wiscombe, W. J.; Weinman, J. A. The delta-Eddington Approximation for Radiative Flux Transfer. *JAS* December **1976**, *33*, 2452.
12. Davies, R. The Effect of Finite Geometry on the Three-dimensional Transfer of Solar Irradiance in Clouds. *JAS* September **1978**, *35*, 1712.
13. Hering, W. S.; Johnson, R. W. *The FASCAT Model Performance Under Fractional Cloud Conditions and Related Studies*; AFGL-TR-84-0168 (ADA169894); December 1984.
14. Hansen, J. E. Exact and Approximate Solutions for Multiple Scattering by Cloudy and Hazy Planetary Atmospheres. *JAS* May **1969**, *26*, 478–487.
15. Potter, J. F. The Delta Function Approximation in Radiative Transfer Theory. *JAS* September **1970**, *27*, 943–949.
16. Lenoble, J. *Atmospheric Radiative Transfer* (ISBN 0-937194-21-2); Deepak Publishing: Hampton, VA, 1993.

17. Wiscombe, W. J.; Joseph, J. H. The Range of Validity of the Eddington Approximation. *ICARUS* **1977**, *32*, 362–377.

18. van de Hulst, H. C., *Multiple Light Scattering, Tables Formulas, and Applications*, v2; Academic Press: NY, 1980.

19. Davies, R. Fast Azimuthally Dependent Model of the Reflection of Solar Radiation by Plane-parallel Clouds. *J. Appl. Opt.* January **1980**, *19*, 250–255.

20. Berk, A.; Bernstein, L. S.; Robertson, D. C. *MODTRAN: A Moderate Resolution Model for LOWTRAN 7*; GL-TR-89-0122, AD A214337; Air Force Research Laboratory: Hanscom AFB, MA, 1989.

21. O'Brien, S. G. *A User Guide for the Deltaed Radiative Transport Model*; ARL-CR-22; December 1992.

22. Lenoble, J., ed. *Radiative Transfer in Scattering and Absorbing Atmospheres: Standard Computational Procedures;* Deepak Publishing: Hampton, VA, 1985.

23. Deirmendjian, D. *Electromagnetic Scattering on Spherical Polydispersions;* Elsevier, 1969.

24. O'Brien, S. G. *Investigation of Relative Strengths of Aerosol Scattering Radiance and Thermal Radiance in the Mid-IR Band*, unpublished white paper, Army Research Laboratory: WSMR, NM, March 2004.

25. Bangert, J. SLAC. http://aa.usno.navy.mil/AA/DoD/software/index.html (accessed verified 2004).

26. Tofsted, D.; Davis, B.; Wetmore, A.; Fitzgerrel, J.; Shirkey, R.; Sutherland, B. *EOSAEL92 Aerosol Phase Function Data Base PFNDAT*; ARL-TR-273-9; June 1997.

27. Shirkey R.; Tofsted, D. *Electro-Optical Aerosol Phase Function Database PFNDAT2004;* ARL-TR-xxxx; 2004 (in press).

28. *U.S. Standard Atmosphere (1976)*; NOAA-S/T76-1562, Supt. of Documents, U.S. Govt. Printing Office: Washington, D.C., 1976.

29. Allen, J. H.; Malick, J. D. The Frequency of Cloud-Free Viewing Intervals. *AIAA 21st Aerospace Sciences Meeting Paper, AIAA-83-0441,* Reno, NV, January 1983.

30. Low, R. D. H.; O'Brien, S.G. *EOSAEL 87 Cloud Transmission Module CLTRAN*; ASL-TR-0221-9; October 1987.

31. Shettle, E. P.; Fenn, R. W. *Models for the Aerosols of the Lower Atmosphere and the Effects of Humidity Variations on Their Optical Properties*; AFGL-TR-79-0214; Air Force Geophysics Laboratory: Hanscom Air Force Base, MA, 1979.

32. MODIS Web. http://modis.gsfc.nasa.gov/ (access verified as of 5 August 2004).

33. *SOLMET, Hourly Solar Radiation-Surface Meteorological Observations*, Vol. 1–Users Manual, (1977), Vol. 2–Final Report (1979); TD-9724; National Climatic Center, NOAA, EDIS, 1979.

Appendix

1. Sample Run from the Text Scenario Using the Input File, visible_input.txt.

```
***  SGR, Transmission, and Radiance Results for Upward looking LOS  ***


>>> Visible band calculation <<<

Haze aerosol type: 2 - Urban

Haze layer thickness (km):   1.000

Met. visible range (km):   2.000

Relative humidity (%):  90.00

 No cloud layers present

Observer local latitude (deg):    32.500

Observer local longitude (deg):   127.000

GMT (hhmm): 0000

Month Day Year:  6  1 2002

Extraterrestrial solar source:
   Zenith angle (deg):   47.283
   Azimuth angle (deg):   89.056

LOS azimuth (deg, E of N):    90.000

LOS zenith (deg):    70.000

Range to target (km):    0.2924

Observer altitude (km AGL):    0.0001

Target altitude (km AGL):    0.1001

Background surface albedo:     0.200
```

Wvlength	W(sensor)	SGR	Tc	T	Lp	Lb(0)
0.350	1.0000	0.6668	0.53345	0.43261	2.4070E+01	6.3618E+01
0.400	1.0000	0.6300	0.58526	0.47063	3.3055E+01	9.9112E+01
0.450	1.0000	0.5880	0.63473	0.50540	4.5875E+01	1.5773E+02
0.500	1.0000	0.5541	0.67713	0.53749	4.8177E+01	1.8798E+02
0.550	1.0000	0.5315	0.71242	0.56835	5.1909E+01	2.2627E+02
0.600	1.0000	0.5196	0.73929	0.59569	5.2298E+01	2.4895E+02
0.650	1.0000	0.5155	0.76070	0.62101	4.8812E+01	2.4987E+02
0.700	1.0000	0.5175	0.77836	0.64505	4.7211E+01	2.5703E+02
0.750	1.0000	0.5248	0.79249	0.66715	4.3769E+01	2.5055E+02

Band-averaged SGR = 0.561

Band-averaged contrast transmission Tc = 0.69043
Band-averaged path transmission T = 0.56038

Band-averaged spectral path radiance Lp = 4.3909E+01 W m-2 sr-1 micrometer-1
Band-averaged spectral bkgrnd radiance Lb(0) = 1.9346E+02 W m-2 sr-1 micrometer-1

Band-integrated path radiance Lp = 1.8063E+01 W m-2 sr-1
Band-integrated bkgrnd radiance Lb(0) = 7.9201E+01 W m-2 sr-1

2. Sample Run from the Text Scenario Using the Input File, mid-ir_input.txt.

*** SGR, Transmission, and Radiance Results for Upward looking LOS ***

>>> Mid-IR band calculation <<<

Haze aerosol type: 2 - Urban

Atmospheric model: 6 - 1976 US Standard

Met. visible range (km): 2.000

Relative humidity (%): 90.00

LOS zenith (deg): 70.0000

Range to target (km): 0.2924

Observer altitude (km AGL): 0.0001

Target altitude (km AGL): 0.1001

Background surface albedo: 0.200

Wvlength	W(sensor)	SGR	Tc	T	Lp	Lb(0)
3.400	1.0000	1.1931	0.78036	0.80913	2.0674E-02	9.0780E-02
3.420	1.0000	1.3029	0.84085	0.87315	1.4535E-02	8.7954E-02
3.440	1.0000	1.4075	0.86493	0.90013	1.2100E-02	8.6080E-02
3.460	1.0000	1.4321	0.86838	0.90429	1.2251E-02	8.9383E-02
3.480	1.0000	1.5129	0.87716	0.91528	1.1448E-02	8.9311E-02
3.500	1.0000	1.5657	0.87944	0.91949	1.1475E-02	9.1034E-02
3.520	1.0000	1.5549	0.87796	0.91794	1.2328E-02	9.6619E-02
3.540	1.0000	1.4999	0.87338	0.91186	1.3947E-02	1.0550E-01
3.560	1.0000	1.4839	0.87092	0.90919	1.5124E-02	1.1224E-01
3.580	1.0000	1.4750	0.87067	0.90850	1.6026E-02	1.1875E-01
3.600	1.0000	1.5143	0.87542	0.91410	1.5813E-02	1.2156E-01
3.620	1.0000	1.5453	0.87869	0.91799	1.5854E-02	1.2510E-01
3.640	1.0000	1.5876	0.88292	0.92291	1.5640E-02	1.2779E-01
3.660	1.0000	1.5761	0.88164	0.92151	1.6702E-02	1.3501E-01
3.680	1.0000	1.4138	0.86096	0.89748	2.2866E-02	1.5776E-01
3.700	1.0000	1.6003	0.88343	0.92383	1.7793E-02	1.4596E-01

Band-averaged SGR = 1.479

Band-averaged contrast transmission Tc = 0.86669
Band-averaged path transmission T = 0.90417

Band-averaged spectral path radiance Lp = 1.5286E-02 W m-2 sr-1 micrometer-1
Band-averaged spectral bkgrnd radiance Lb(0) = 1.1130E-01 W m-2 sr-1 micrometer-1

Band-integrated path radiance Lp = 4.5069E-03 W m-2 sr-1
Band-integrated bkgrnd radiance Lb(0) = 3.3249E-02 W m-2 sr-1

3. Sample Run from the Text Scenario Using the Input File, far-ir_input.txt.

*** SGR, Transmission, and Radiance Results for Upward looking LOS ***

>>> Far-IR band calculation <<<

Haze aerosol type: 2 - Urban

Atmospheric model: 6 - 1976 US Standard

Met. visible range (km): 2.000

Relative humidity (%): 90.00

LOS zenith (deg): 70.0000

Range to target (km): 0.2924

Observer altitude (km AGL): 0.0001

Target altitude (km AGL): 0.1001

Background surface albedo: 0.200

Wvlength	W(sensor)	SGR	Tc	T	Lp	Lb(0)
10.400	0.1000	1.6081	0.91647	0.94636	4.3319E-01	5.0224E+00
10.420	0.2000	1.5797	0.91461	0.94420	4.5055E-01	5.1113E+00
10.440	0.3000	1.5911	0.91612	0.94558	4.3921E-01	5.0728E+00
10.460	0.4000	1.5240	0.91366	0.94162	4.7109E-01	5.2944E+00
10.480	0.5000	1.4951	0.91203	0.93940	4.8882E-01	5.3949E+00
10.500	0.6000	1.5362	0.91472	0.94279	4.6130E-01	5.2485E+00
10.520	0.7000	1.5784	0.91701	0.94577	4.3706E-01	5.1061E+00
10.540	0.8000	1.4692	0.91198	0.93835	4.9665E-01	5.4837E+00
10.560	0.9000	1.4648	0.91207	0.93825	4.9728E-01	5.4979E+00
10.580	1.0000	1.5375	0.91501	0.94303	4.5856E-01	5.2354E+00
10.600	1.0000	1.5638	0.91680	0.94515	4.4134E-01	5.1452E+00
10.620	1.0000	1.5448	0.91596	0.94394	4.5087E-01	5.2059E+00
10.640	1.0000	1.5457	0.91602	0.94401	4.5007E-01	5.2007E+00
10.660	1.0000	1.5629	0.91731	0.94547	4.3813E-01	5.1409E+00
10.680	1.0000	1.5631	0.91749	0.94560	4.3688E-01	5.1376E+00
10.700	0.5000	1.5526	0.91756	0.94529	4.3907E-01	5.1696E+00

Band-averaged SGR = 1.539

Band-averaged contrast transmission Tc = 0.91540
Band-averaged path transmission T = 0.94329

Band-averaged spectral path radiance Lp = 4.5646E-01 W m-2 sr-1 micrometer-1
Band-averaged spectral bkgrnd radiance Lb(0) = 5.2337E+00 W m-2 sr-1 micrometer-1

Band-integrated path radiance Lp = 9.7792E-02 W m-2 sr-1
Band-integrated bkgrnd radiance Lb(0) = 1.1205E+00 W m-2 sr-1

Acronyms

AGL	above ground level
ARL	U.S. Army Research Laboratory
ANSI	American National Standards Institute
AFGL	Air Force Geophysics Laboratory
ASCII	American Standard Code for Information Interchange
CASTFOREM	Combined Arms and Support Taskforce Evaluation Model
CFLOS	cloud free line-of-sight
CLTRAN	Cloud Transmission
EOSAEL	Electro-Optical Systems Atmospheric Effects Library
FASCAT	Fast Atmospheric Scattering
GMT	Greenwich Mean Time
GUI	graphical user interface
MODIS	Moderate resolution Imaging Spectroradiometer
MODTRAN	Moderate Transmission
PFNDAT	Phase Function Data base
IR	infrared
LOS	line-of-sight
SGR	Sky-to-Ground Ratio
SLAC	Solar-Lunar Almanac Core
TOA	top of atmosphere
V&V	verification and validation

Distribution

	Copies
Army Research Laboratory Attn: AMSRD-ARL-D 2800 Powder Mill Road Adelphi MD 20783-1197	1
Army Research Laboratory Attn: AMSRD-ARL-CI (Dr. Gantt) 2800 Powder Mill Road Adelphi MD 20783-1197	1
Army Research Laboratory Attn: AMSRD-ARL-RO-EN (Dr. Bach) PO Box 12211 Research Triangle Park, NC 27009	1
Army Research Laboratory Attn: AMSRD-ARL-CI-EI (Dr. Shirkey) WSMR NM 88002-5501	4
Army Research Laboratory Attn: AMSRD-ARL-CI-EW (Dr. O'Brien) WSMR NM 88002-5501	4
Army Research Laboratory Attn: AMSRD-ARL-CI-EW (D. Tofsted) WSMR NM 88002-5501	1
Army Research Laboratory Attn: AMSRD-ARL-CI-CT (P. Jones) APG, MD 21005-5067	1
Army Research Laboratory Attn: AMSRD-ARL-SL-BB (R. Sandmeyer) APG, MD 21005	1
Army Materiel Systems Analysis Activity Attn: AMXSY-SC (J. Mazz) 392 Hopkins Road APG MD 21005-5071	1
Army Materiel Systems Analysis Activity Attn: AMXSY (R. Kistner) 392 Hopkins Road APG MD 21005-5071	1
US Army Night Vision & Electronic Sensors Directorate Performance Model Development Branch Attn: AMSRD-CER-NV-MS-PMD (T. Maurer) 10221 Burbeck Rd Ft. Belvoir, VA 22060-5806	1
US Army Night Vision & Electronic Sensors Directorate Performance Model Development Branch Attn: AMSRD-CER-NV-MS-PMD (J. Hixson) 10221 Burbeck Road Fort Belvoir, VA 22060-5806	1
Army Modeling & Simulation Office DA G37 (DAMO-SBM) 400 Army Pentagon Washington, DC 20310-0450	1
Director, USA TRADOC Analysis Center Attn: ATRC-W (D. Vargas) WSMR, NM 88002-5502	1
Director, USA TRADOC Analysis Center Attn: ATRC-WBC (D. Dixon) WSMR, NM 88002-5502	1
Director, USA TRADOC Analysis Center Attn: ATRC-WEA (D. Mackey) WSMR, NM 88002-5502	1
Director, USA TRADOC Analysis Center Attn: ATRC-WS (A. Kientz) WSMR, NM 88002-5502	1

	Copies
Director, USA TRADOC Analysis Center Attn: ATRC-WJ (S. Gray) WSMR, NM 88002-5502	1
Director, USA TRADOC Analysis Center Attn: ATRC-WG (Dr. E. George) WSMR, NM 88002-5502	1
Director, USA TRADOC Analysis Center Attn: ATRC-WE (W. Butler) WSMR, NM 88002-5502	1
Director, USA TRADOC Analysis Center Attn: ATRC-WEC (D. Durda) WSMR, NM 88002-5502	1
Director, USA TRADOC Analysis Center Attn: ATRC-WB (P. Jones) WSMR, NM 88002-5502	1
Director, USA TRADOC Analysis Center Attn: ATRC-WA (L. Southard) WSMR, NM 88002-5502	1
Director, USA TRAC-FLVN Attn: ATRC-FM (T. Bailey) 255 Sedgwick Ave Ft Leavenworth, KS 66027-2345	1
Director, USA TRAC-FLVN Attn: ATRC-FMD (H. Jones) 255 Sedgwick Ave Ft. Leavenworth, KS 66027-2345	1
Director, USA TRAC-FLVN Attn: ATRC-FMD (M. Adkins) 255 Sedgwick Ave Ft. Leavenworth, KS 66027-2345	1
Director, USA TRAC-FLVN Attn: ATRC-FMA (T. Gach) 255 Sedgwick Ave Fort Leavenworth KS 66027-2345	1
Director, USA TRAC-FLVN Attn: ATRC-FMA (S. Glasgow) 255 Sedgwick Ave Ft Leavenworth, KS 66027-2345	1
Director, USA TRAC-FLVN Attn: ATRC-FR (P. Blechinger) 255 Sedgwick Ave Ft Leavenworth, KS 66027-2345	1
Director, USA TRAC-FLVN Attn: ATRC-F (COL J. Appleget) 255 Sedgwick Ave Ft Leavenworth, KS 66027-2345	1
Director, USA TRAC-FLVN Attn: ATRC-FJ (W. Krondak) 255 Sedgwick Ave Ft Leavenworth, KS 66027-2345	1
Director, USA TRAC-FLVN Attn: ATRC-FW (E. Boehner) 255 Sedgwick Ave Ft Leavenworth, KS 66027-2345	1
ERDC/CRREL Attn: Dr. G. Koenig 72 Lyme Rd Hanover, NH. 03755	1
Army Corps of Engineers Topographic Eengineering Center Data and Signature Analysis Branch Ft. Belvoir, VA 22060	1
U.S. Military Academy Dept of Mathematical Sciences Thayer Hall West Point, NY 10996-1786	1
U.S. Military Academy Combat Simulation Laboratory (Dr. P. West) West Point, NY 10996	2

Copies

USA PEO STRI 1
Advanced Simulation Concepts Division (ED)
L. Curless
12350 Research Pkwy
Orlando, FL 32826-3276

USA PEO STRI 1
FCS Training IPT Environment
D. Stevens
12350 Research Pkwy
Orlando, FL 32826-3276

USA PEO STRI 1
Project Manager Constructive Simulation
R. A Copeland
12350 Research Pkwy
Orlando, FL 32826-3276

USA PEO STRI 1
Project Manager Constructive Simulation
G. Manross
12350 Research Pkwy
Orlando, FL 32826-3276

USA PEO STRI 3
Project Manager Constructive Simulation
B. S. Hirtle
12350 Research Pkwy
Orlando, FL 32826-3276

PEO STRI 1
Project Manager Constructive Simulation
LTC William Blackledge
12350 Research Parkway
Orlando, FL 32826-3276

PEO STRI 2
Project Manager Constructive Simulation
LTC John Surdu
12350 Research Parkway
Orlando, FL 32826-3276

Copies

AFRL/IFOIL 1
525 Brooks Road
Rome, NY 13441-4505

Air Weather Service 1
Tech Library FL4414 3
Scott AFB IL 62225-5458

HQ USAFA/DFLIB 1
2354 Fairchild Drive, Suite 3A10
USAF Academy, CO 80840-6214

Tech Connect 1
AFRL/XPTC
Bldg 16, Rm 107
2275 D Street
WPAFB OH 45433-7226

Dr. Andy Goroch 1
Naval Research Laboratory
Marine Meteorology Division
Code 7543
7 Grace Hopper Ave
Monterey, CA 93943-5006

U.S. Naval War College 1
War Gaming Department (Code 33)
686 Cushing Road
Newport, Rhode Island 02841-1207

Space and Naval Warfare Systems Center 1
C. McGrath, Code 2858
53560 Hull Street
San Diego, CA 92152-5001

Naval Postgraduate School 1
J. D. Eagle
OR/Er
1 University Circle
Monterey, CA 93943

	Copies
Naval Postgraduate School R. K. Wood OR/Wd 1 University Circle Monterey, CA 93943	1
Naval Postgraduate School G. Schacher Dept. of Physics 1 University Circle Monterey, CA 93943	1
Naval Postgraduate School W. B. Maier II Dept. of Physics 1 University Circle Monterey, CA 93943	1
Ruth H. Hooker Research Library 4555 Overlook Ave, SW Washington, DC 20375	1
J. Bangert Head, Astronomical Applications Dept U.S. Naval Observatory 3450 Massachusetts Ave., NW Washington, DC 20392-5420	1
JWARS Attn: C. Burdick 1555 Wilson Boulevard, Suite 619 Arlington, VA 22209	1
Northrop Grumman Information Technology Melanie Gouveia 55 Walkers Brook Dr. Reading, MA 01867	1
Northrop Grumman Mission Systems Don Timian 5502 Leesburg Pike, Suite 1200 Falls Church, VA 22041	1
Technical Reports Boulder Laboratories Library, MC 5 325 Broadway Boulder, CO 80305	1
NCAR Library Serials National Center for Atmospheric Research PO Box 3000 Boulder, CO 80307-3000	1
U.S. Army Research Laboratory Attn: AMSRD ARL CI IS R Mail & Records Mgmt Adelphi, MD 20783-1197	1
Admnstr Defns Techl Info Ctr Attn: DTIC OCP (W Smith) 8725 John J Kingman Rd., Ste. 0944 Ft Belvoir, VA 22060-6218	1 (CD only)
US Army Research Laboratory AMSRD ARL CI OK TL 2800 Powder Mill Rd. Adelphi, MD 20783-1197	2
TOTAL	75

INTENTIONALLY LEFT BLANK.